FEMTOSECOND LASER PULSE-INDUCED STRUCTURAL MODIFICATION OF LANTHANUM ALUMINOSILICATE GLASSES: REFRACTIVE INDICES IN VISIBLE VS. TERAHERTZ FREQUENCY REGIONS

BY

DAVID KOTARO DOBESH

A THESIS
SUBMITTED TO THE FACULTY OF

ALFRED UNIVERSITY

IN PARTIAL FULFILLMENT OF THE REQUIREMENTS
FOR THE DEGREE OF

MASTER OF SCIENCE

IN

GLASS SCIENCE

ALFRED, NEW YORK

April, 2019

FEMTOSECOND LASER PULSE-INDUCED STRUCTURAL MODIFICATION OF LANTHANUM ALUMINOSILICATE GLASSES: REFRACTIVE INDICES IN VISIBLE VS. TERAHERTZ FREQUENCY REGIONS

BY

DAVID KOTARO DOBESH

B.A. HASTINGS COLLEGE 2016

SIGNATURE OF AUTHOR_____

APPROVED BY_____

S.K. SUNDARAM, ADVISOR

_____

ALEXIS CLARE, ADVISORY COMMITTEE

_____

WILLIAM LACOURSE, ADVISORY COMMITTEE

_____

WILLIAM M. CARTY, CHAIR, ORAL THESIS DEFENSE

ACCEPTED BY_____

GABRIELLE G GAUSTAD, DEAN
KAZUO INAMORI SCHOOL OF ENGINEERING

ACKNOWLEDGMENTS

Firstly I would like to thank my family for their never ending support and helpfulness throughout my years. I would additionally like to thank my adviser Dr. Sundaram for his guidance and in my career and this endeavor. I also would like to thank my committee members Dr. Clare and Dr. LaCourse for their support and insight. I also appreciate the time and support from the many professors at Alfred University who have expanded and contributed to my learning experience in one form or another. I am especially thankful for the glass community at Alfred University in the arts and sciences who have provided an unique experience and opportunity to expand my experiences with glass. I would also like to thank the generosity of the people at Corning Inc. who have help collaborate and spent time in collecting data for this work. I would also like to thank my friends and cohorts who have personally encouraged me through my studies and have provided mental support. I would also like to thank the school of engineering and staff for helping me with scheduling and time spent in handling all the necessary administrative work. I would also like to extend my gratitude to the community of Alfred University and the village of Alfred. To the many people who provided the Alfred experience and maintain the unique and exquisite opportunity to attend and live in this beautiful area, outside of ordinary.

TABLE OF CONTENTS

Page

LIST OF TABLES

Page

LIST OF FIGURES

Page

ABSTRACT

Lanthanum aluminosilicate (SAL) glasses are of interest due to their superior physical and chemical properties. The large glass forming region allows for incorporation of rare-earth elements for expanded and detailed tuning of glass properties. Lanthanum inclusions within the aluminosilicate network increase the refractive index based on the concentration. The amount of lanthanum can be tailored to develop optical materials with a corresponding third-order susceptibility applicable for non-linear optical applications. A novel method for altering the base glass refractive index utilized femtosecond laser modification, where the timescale of the pulse duration permits structural alterations in a locally defined volume for the modification of optical components. We studied femtosecond laser modifications of SAL glasses with 11-23 mol% La_2O_3 content. Refractive indices of these glasses in the visible and the terahertz frequencies were measured and correlated to change in glass structure. The role of lanthanum was compared to traditional glass modifiers within the glass structure in terms of polarizability and optical basicity for femtosecond laser refractive index modification. ^{27}Al Magic Angle Spinning Nuclear Magnetic Resonance (MAS-NMR) was used to identify Al-speciation within the SAL glasses. We used terahertz time-domain spectroscopy (THz-TDS) for THz refractive index measurements. Our results show a linear correlation between refractive index measurements in visible and terahertz frequencies. In addition, our results demonstrate that THz-TDS can be possible means of extending the detectable limits in refractive index measurements of disordered glass structures.

I. INTRODUCTION

Rare earth oxide additions to glasses are of great interest due to their inherent optical magnetic properties leading towards technological advances in material response and behavior. The concentration of rare earth oxides within glasses can be advantageous due to the additive behavior as well as dopant levels which will significantly alter the glass properties and morphology. Aluminosilicate glasses exhibit properties which have been found to be advantageous for a wide variety of uses within the sciences and engineering which propel technological innovation. Applications of the aluminosilicates have been founded on their superior physical (e.g. high micro hardness and elastic modulus)[1-3] and chemical durability. The aluminosilicate glasses also provide exceptional solubility of rare-earth elements (REE) which allow for higher content inclusion for a greater range of applications.

The inclusion of a rare-earth elements, as the active component within the aluminosilicate glass network, expand on the superior qualities of aluminosilicates for new laser system materials and optical telecommunication systems[3,4]. Common additions of traditional mono- or/and di-valent alkali/akali earth elements to the aluminosilicates differ from the REEs partially due to the tri-valent state and higher cation field strength of the REE. Lanthanide inclusions are of interest for high-power laser applications[5], optical switch systems[6,7]. The role of lanthanum oxide (La_2O_3) of the VI period in the aluminosilicate glass system will be focus of this thesis.

The advent of ultra-fast pulse femtosecond (fs) lasers with applications of modification of optical glasses and dielectric materials has developed new research areas for waveguides, time delay spectroscopy, Bragg gratings, and three dimensional memory[4,8-14]. Fs-laser modification of solid dielectric materials allows for precise modification of materials, spatially as well as and temporally. Pulse or pulse train applications can then incur greater peak energy deposition.

1. Lanthanum Aluminosilicate Glasses

The base composition of aluminosilicate glasses has been selected due to its inherent chemical stability and solubility of REE. The inclusion of La_2O_3 to silica (SiO_2) and alumina (Al_2O_3) forms the ternary glass system of SAL glasses. Aluminosilicate glasses exhibit liquid immiscibility in their phase diagrams for REE oxides (R_2O_3) where broad regions are formed from less than 1 mol% and to the upper regions of 20 mol%[15]. The mol% of each component was chosen within the ternary glass forming region. The concentration of the traditional network former of silica will contain the largest mol% in the ternary system for forming the glass structural units within the glass forming region.

Silica melting temperature was taken into consideration for the upper limit of the melting furnace, where high concentrations of silica requires melting beyond the limit of the refractory, as well as the platinum crucible. Industrial use of silica in the form of fused quartz or vitreous fused silica is primarily selected based on its superior thermal and optical properties with a high glass transition temperature and low coefficient of thermal expansion.

The optical transmittance also displays a wide range from UV to IR wavelengths. Difficulty arises in developing bulk amorphous binary alumina specimens[16], but Al_2O_3 within the SAL glass systems plays an intriguing role as an intermediate, having both network former and modifier characteristics. The alumina polyhedral species will form 4,5, and 6-fold coordination species with oxygen atoms. The amount of alumina was taken to be 22mol%. The rather high concentration is due to the glass forming regions of the SAL glass systems to ensure incorporation of lanthanum since $La_2O_3-SiO_2$ alone will form extensive regions of liquid immiscibility[17]. Alumina speciation will be dependent on the La/Al ratio. REE additions to silicate and aluminosilicate glasses have been investigated for active fibers in laser operations for continuous or pulsed modes[6].

Comparing to traditional glass modifiers such as alkali or alkali earths, the lanthanides decrease the electrical conductivity, but increase the refractive index, elastic moduli, and glass transition behavior. The aluminosilicate glasses contain REE with their trivalent-ion valency and stronger field strength, have seen greater technological and telecommunications applications[4,18,19], where REE ions have been beneficial in providing unique optical and electrical properties within glasses compared to traditional modifier ions

(e.g., Na^{+}, K^{+}, $Ca^{(2+)}$). Trivalent REE elements contain a higher cation field-strength (CFS), creating a stronger cross-linking within the structural framework fragments from REE polyhedra within the glass network[20]. The exclusion of traditional modifiers, which have a high mobility within the aluminosilicates[10], also increase the hardness[1] and chemical durability[19] of the SAL glasses. The production and manufacturing of these glasses have already seen an increase in demand and production with similar industrial practices to soda-lime-silicates.

In comparison with chalcogenide glasses the broadband transmission window, with the near to far-infrared electromagnetic waves, are narrower with the inclusion of oxygen. However, the chemical durability and hardness of aluminosilicates is superior with common oxide batching and production procedures with viable applications for durable high power and radiation environments. In addition, the increasing need for smaller optics are also of interest for compact devices in defense and transportable equipment will find applications for high refractive index components.

2. Polarizability

Employing the view of polarizability and optical basicity, the Lorentz-Lorenz equation can be utilized to correlate the optical basicity from experimental data of refractive indices and the energy band gap. The refractive index from calculations and use of the sodium line by Duffy et al.[21-23] are suitable, since the molar polarizability calculated from strictly at infinite wavelength is estimated. Specifically for isotropic materials and disordered homogeneous dielectrics such as glasses, the molar polarizability can be calculated using the Lorentz-Lorenz relationship in equation 1, where α_m is the mean polarizability. The molar volume V_m of a compound and its corresponding refractive index at 589nm yield the average molar refraction of isotropic substances. Further expansion of polarizability of glasses, proposed by Duffy and Ingram[24] correlated the electron density carried by oxygen in terms of basicity termed optical basicity, based on the Lewis acid-base properties of oxides and glasses. Dimitrov and Sakka[25] determined the average electronic polarizability for simple oxides using the experimental linear refractive index and energy gap proposed by Duffy and Ingram[24].

Increases in the linear refractive index with La_2O_3 concentration and correspondingly the nonlinear refractive index may be estimated by the polarizability through optical basicity. Therefore, applications in optoelectronics technology for modification of components will be of great interest for optical networks as well as miniaturized optical components with high contrast refractive index modifications. In terms of optical basicity, the acid-base properties can be correlated to the oxide polarizability and coordination number for aluminosilicates quantitatively[26,27].

$$\alpha_m = \frac{3V_m}{4\pi N}\frac{n^2-1}{n^2+2} \tag{1}$$

In our modern age the transfer of information had increased with a sharp demand for the amount and transfer speed. New materials will meet this demand and increase the bandwidth necessary to fill the need of every growing communication networks. Photon-based systems allow the ultra-high-speed transfer via photonic systems which provide unparalleled speed. One aspect of the photonic systems requires nonlinear optical

properties. The optical response of a material, to an applied intensity of an electric field, is based on the dielectric polarizability of ions[21]. Optical nonlinearity from the third-order susceptibility be correlated to the polarizability of oxide ions where it is possible to relate the polarizability to optical basicity.

The optical basicity was proposed by Duffy and Ingram[24] to correlate the electron density carried by oxygen in terms of basicity based on the acid-base properties of glasses and oxides. Further research on optical basicity has been followed by calculating the average electronic polarizability for simple oxides by Demitrov and Sakka[27] measuring the linear refractive index and energy gap on the basis of the Lorentz-Lorenz equation. Addition of lanthanum oxide to glasses have shown to increase the linear refractive index with increasing concentration[19,28] and correspondingly the nonlinear refractive index[6]. REEs have displayed the lanthanide contraction phenomenon where the electronic polarizability of an oxide ion decreases with increasing atomic number of the cation[29]. Results of determining the electronic polarizability based on the atomic number of lanthanides by Zhao et al.[22] have displayed this phenomenon.

Rare earth oxides within aluminosilicates correspondingly show physical properties such as the density, glass transition temperature, elastic moduli, and hardness increase, while the thermal expansion coefficient and molar volume reduces as the cation field strength decreases with radius increase. Aluminosilicates also show a stronger dependence on the CFS of the REEs in ternary systems. The percentage of coordinated alumina species will deviate from the tetrahedral configuration as atomic number of the lanthanide series increase. The trend is that the higher coordinated AlO_5 and AlO_6 polyhedral concentrations increase with the CFS of the lanthanide[30-32].

Aluminosilicate base glasses were investigated for their accumulative polarizability with cation inclusions, for estimated optical basicity with insights of the glass structure and material response. The results displayed that the majority of the polarizable ions within the glass could be estimated in terms of the oxygen atoms[33,34]. By isolating the additive cation contributions and estimating the average state of the electron clouds of the oxygen atoms after they contribute to chemical bonding, the resulting optical basicity may lead to an optimization of glasses. The third-order susceptibility response to an applied electric field can be evaluated by the polarization response of the glass network, where bridging oxygens

(BO) in the structural framework may be correlated to non-bridging (NBO) of tetrahedral units.

Oxygen polarizability within the glass network may dictate the level of response by the distortion of the dipole configuration to an external electric field. The optical basicity takes into account the degree of the oxygen contribution to the electronegativity being able to estimate and correlate the optical basicity with the polarizability beforehand for optimization. Extending the optical basicity to aluminosilicates, we can gather further estimated polarizability from coordination states. The investigation of aluminum oxide is an important and useful role since the coordination number will change with composition, compared to silicon oxide in the tetrahedral configuration. Alumina species have been found to be in various coordination arrangements within glasses with predominantly 4-fold coordination but will also occur in 5 and 6-fold coordination. The percentage of the coordination number in aluminosilicate have been measured using 27Al MAS-NMR[30,35-37]. In terms of optical basicity, the acid-based properties can correlate the oxide polarizability with the coordination number for aluminosilicates[26]. By identifying structural changes within aluminosilicates when can use the optical basicity with a comprehensive study of the optical refractive index to estimate the average polarizability from the oxygen electron for new optical material developments.

The aluminosilicate glasses are investigated for their polarizability with optical basicity, where majority of the polarizable ions can be estimated in terms of the oxygen atoms[26]. This is in part due to the perspective of investigating the average state of the electron clouds of the oxygen atoms after they contribute to chemical bonding. The state of the oxygen electron clouds with bridging (BO) and non-bridging oxygens (NBOs), can be estimated by the distortable state of the polarizability. The optical basicity estimation takes into account the degree of the negatively charged oxygen contribution to the electronegativity within the glass matrix and which can correlate the optical basicity with the polarizability.

3. 27Al Magic Angle Spinning Nucular Magentic Resonace (MAS NMR)

Aluminosilicate glass systems have been investigated by 27Al Magic Angle Spinning Nuclear Magnetic Resonance (MAS-NMR) for defining the local coordination number of the Al-species. The structural implications is that the aluminum species can act as a glass intermediate with network forming behavior and modifier characteristics within the glass matrix. The fundamentals of NMR are based on the nuclear particle spin with an inherent magnetic moment. To determine the coordination numbers of specific cations within glass, NMR characterization method studies transitions between energy levels of the nuclear magnetic moment. When magnetic moment of a particle is placed within a magnetic field, the applied field creates a torque causing the magnetic moment to rotate and a splitting of degenerate nuclear spin levels due to the Zeeman interaction. Thus, the nucleus serves as a probe and provides information on the immediate surroundings. The precession of the magnetic moment creates a detectable voltage from Faraday's Law. The collected voltage can provide information about the system through deviation of the angular momentum with torque from the magnetization[38].

Solid state NMR techniques are employed to resolve the broad spectrum of the effects due to anisotropic interactions. However, pioneering work by Andrew and Lowe[39] discovered that the anisotropic dipolar interactions could be suppressed using the artificial motions of the sample by rotating about an axis at 54.74° with respect to the applied magnetic field. Rotating at this angle with NMR is now referred to as magic-angle spinning (MAS). Using this angle in combination with spinning at a velocity at or above the dipolar linewidth enables minimization of large anisotropic NMR interactions between nuclei and increase of the signal to noise ratio. This reduces the magnitude of multiple spinning sidebands by localizing the signal compared to spreading over the entire breadth of the spectrum in NMR spectra. The gathered splitting and energy states are expressed as the nuclear Hamiltonian which includes terms for the Zeeman splitting, chemical shift, and dipolar and quadrupolar terms.

Through 27Al MAS-NMR of aluminosilicate glasses it is possible to resolve the Al coordination species of the short-range order. The characterization is only specific to detection of Al-species within the glass structure. Structural studies of aluminosilicates would ideally include 29Si MAS-NMR and 17O MAS-NMR. In multicomponent glasses

29Si MAS-NMR has been used to determine Q-species of the tetrahedral units from the observed chemical shift in the spectrum. However, the 29Si NMR chemical shift center of gravity exhibit, rather featureless peaks with nominal resolved signals from various tetrahedral units[40]. Presence of shielding effects from neighboring NBOs and the number of oxygen linked nearest neighbor Al atoms with respect to the Si tetrahedron. 29Si MAS-NMR of aluminosilicate glasses generally exhibit featureless peaks since the RE-Si-Al-O have scarcely resolved signals from Q-species of various of Si[40].

4. Terahertz Time-Domain Spectroscopy (THz-TDS)

Vibrational spectroscopy methods, infrared (IR) and Raman spectroscopy, have been used to study laser pulse-induced structural changes in glasses. However, vibrational analysis of glass below 3 THz is hindered by the large noise and broad features of IR and Raman techniques. THz-TDS has been proposed as an enhanced method for determining low-energy excitations within glasses[41,42]. Early reports on refractive index measurements in THz regime have shown an increased distinction between silicate glasses from 0.1 to 2.0 THz[43], where the increase of scale in the THz regime allow for greater discernibility between refractive indices. Silicate glass refractive index measurements have shown promising features in the frequency response for coherent terahertz time-domain spectroscopy (THz-TDS) measurements.

Previous reports by Naftaly et al.[8,43,44] have shown that refractive index of glasses measured using THz-TDS have shown a linear correlation between visible and THz refractive indices. Moreover, the linear trend is correlated to network modifiers, where fused silica and Pyrex deviate from the linear correlation[45]. The increased oxygen polarizability within the network will also a greater detection limit for THz-TDS spectroscopy[44]. THz measurements allow for an alternative and efficient characterization technique on disordered systems and a non-destructive testing method. The high penetration in THz depth of allows for submillimeter spatial resolution[46]. THz-TDS collection allows for extraction of dispersion properties with minimal collection time from phase and amplitude signals from the propagated electromagnetic wave. In the present thesis, we present our data that provide a correlation between the glass structure and visible and the THz properties of the target glasses.

5. Femtosecond laser Irradiation

Material response to laser irradiation has been investigated lately due to the advent of high-power laser systems. The response is governed by two basic factors; the type of material and laser source; material can be compositionally tailored to induced optimal response to a specific laser source. Investigation has been done with a wide range of materials such as plastics, glasses, and crystals. Our focus will be on the glassy state of lanthanum aluminosilicates. Multiple component glasses have been used to see the response of the material to femtosecond laser modification; femtosecond laser irradiation has been found to be instrumental in the development of micro-fabrication photonics by modifying specific regions in transparent glasses for waveguide, gratings, and optical amplifier technology[18,47].

The timescale of material interactions have been determined in molecules and atoms, where the duration of femtoseconds will be in the range of the period of their oscillations[48]. The development of femtosecond laser pulses has been utilized in spectroscopic observation of materials and laser processing of materials. The ultrafast femtosecond laser modification and processing of materials deviate from slower timescale pulse durations mainly from minimal thermal effects[48]. Nanosecond duration of laser pulses have been shown to deposit predominantly thermal energy leading to ablation and evaporation, and thermal diffusion due to the pulse duration. The shorter pulse duration from femtosecond lasers allow modification of the materials through alterations of interatomic forces which modify the band structure of the material through multiphoton absorption without increasing the thermal energy[48]. One aspect of femtosecond laser modification is the repetition rate of the pulses for locally modification of the glass structure for induced refractive index changes. Lower repetition rates of a femtosecond laser pulse permit individual pulses. Higher repetition rates above 200kHz increase the thermal diffusion time from shorter time lengths between following pulses[12] which allow for permanent modifications and faster writing speeds leading to an increase in processing time. Due to the fixed repetition rate used in this study the variable rastering speed of the laser will allow for the modified volume of the laser pulses to be controlled through irradiation time by the number of successive pulses.

The femtosecond (fs) laser pulses can be utilized to modify highly localized regions both spatially and temporally[13] with the rastering rate. The pulse duration and repetition rate of fs-lasers allow photo-induced refractive index alterations due to the high energy density, multiphoton and nonlinear response of glasses[49]. The timescale of fs pulses will allow greater precision in locally confined areas than longer pulses, which will allow for higher induced energy with minimal contributions to the thermally induced ablation process[48]. SAL glasses are of interest for fs modification due to their high optical damage threshold and substantial polarizability to induce linear and nonlinear refractive index modifications. The compositional dependence of fs-laser modification can also be coupled to the magnitude and uniformity of refractive index alterations[11], which allows for efficient and precise tailoring of optical materials. Localized changes within the glasses can sequentially be altered permanently by a structural change of the dielectric material with laser fs-laser pulses though nonlinear photon absorption process.

II. EXPERIMENTAL PROCEDURE

1. Glass Synthesis and Sample Preparation

High-purity (Alfa Aesar) chemicals were used to synthesize four SAL glass batches. The compositional range altered the lanthanum and silica content with alumina being constant ranging from (55-67mol%)SiO_2-22mol%Al_2O_3-(11-23mol%)La_2O_3. High-alumina content was selected from the glass forming region of the ternary SAL system depicted in Figure 1. Glass forming region of reported lanthanum aluminosilicates[2,3,15,19,50,51] with specimens of investigation highlighted within the glass forming regions based on experimental reported values. The high-alumina concentration helped dissolution of lanthanum oxide into the glass avoiding phase separation.

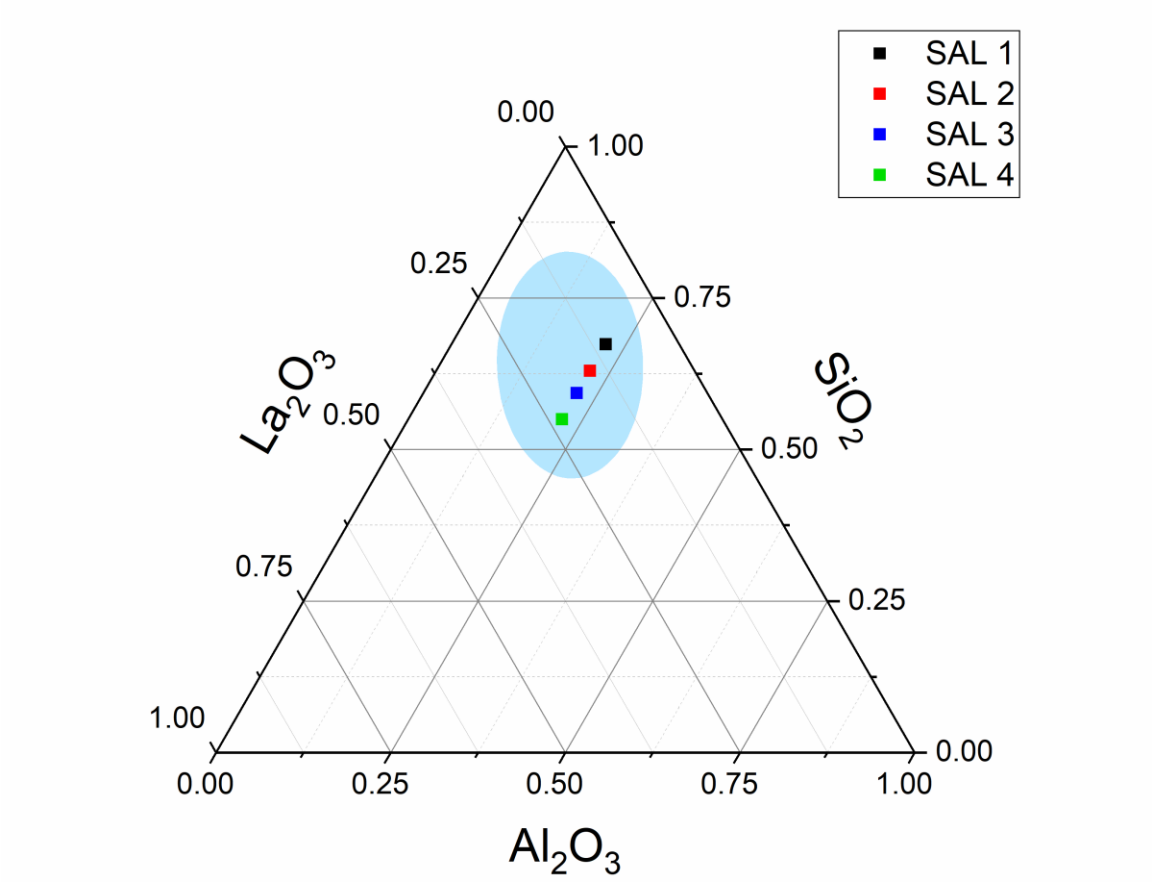

Figure 1. Glass forming region of reported lanthanum aluminosilicates[2,3,15,19,50,51] with specimens of investigation highlighted

Batch size of 50 g was melted conventionally in a discontinuous two-step process. Raw materials were dry milled without media to ensure uniform mixing and reduced contaminates. The first melt stage was done in a 95Pt-5Rh Wt% crucible in air atmosphere at 1600-1650°C for 12h then poured into deionized water to quench and frit the glass. Glass frit was then powdered to ensure uniform particle size. Then the glass powder melted for a longer period at 1600-1650°C for 19-22h in a 95Pt-5Rh Wt% crucible under air to ensure a homogenous glass without striae and seeds. Table I shows the SAL glass sample compositions.

Table I - Lanthanum Aluminosilicate glass compositions

Glass Specimen	**La_2O_3 mol %**	**Al_2O_3 mol%**	**SiO_2 mol%**	**Molar Volume (cm^3)**	χ_{Si}	χ_{Al}	χ_{La}
SAL1	11	22	67	2912.85	0.504	0.331	0.165
SAL2	15	22	63	2902.29	0.460	0.321	0.219
SAL3	19	22	59	2943.16	0.418	0.312	0.270
SAL4	23	22	55	2997.48	0.379	0.303	0.317

χ_n is the cation total ratio of the compositions.

2. Sample Preparation

Glass melt was poured into a two-part cylindrical graphite mold and allowed to cool to room temperature. Glasses were then annealed from room temperature to 950°C for a 2h dwell period then cooled at 1.5°C/min to room temperature. Samples were viewed through a polariscope to visually examine the birefringence to ensure internal stresses were removed. Bottom sections were cut from the glass ingot and polished to 25nm diamond suspension with a sample thickness of 0.78-1.19mm.

3. Glass Characterization

3.1 Differential Scanning Calorimetry (DSC)

DSC measurements were used (SDT-Q600, TA Instruments, Newcastle, DE, USA) to determine the glass transition temperature (T_g). A heating rate of 20°C/min up to 1500°C was used for all tests in flowing air. Platinum pans were used and the heat flow integrations automatically normalized using the dynamic weight at the beginning of the phase transition. Glass powders retrieved from the bulk SAL-glass compositions after annealing were used for the measurements. The T_g-values were estimated from the onset temperature of the endothermic slope.

3.2 Ultraviolet-Visible (UV-Vis) Spectroscopy

Absorption spectra of the glass samples in the UV, Vis, and near-infrared (IR) range were collected using a LAMBDA 950 UV-Vis spectrometer (Perkin Elmer, Waltham, MA, USA). The wavelength range was 200-900nm with a step size of 1nm and the scans were conducted at room temperature in air. The indirect band gaps of the SAL-glasses were estimated using the Tauc plot of the UV absorption edge and extrapolating from the tangent edges to the intercept for estimation in eV energy contribution from phonons.

3.3 Optical Refractive Index

Visible refractive index measurements were performed using a Metricon Model 2010 (Metricon Corporation, Pennigton, NJ, USA). Prism Coupler at 406nm, 473nm, 532nm, 633nm, 790nm, and 981nm using various laser sources. Each sample was coupled to the prism and evaluated for sharpness of the measured "knee" at that location. Sharpness of the knee is dependent upon glass homogeneity and surface quality (flatness and roughness) at the coupled region. If necessary, the sample was repositioned until a sharp knee was obtained. Without moving the sample, measurements were performed at each wavelength to determine refractive index dispersion. For each glass sample, the measured indices of refraction results were fitted to Sellmeier and Cauchy dispersion equations and the constants determined. The instruments used for measurements are calibrated periodically according to ASTM recommended procedures using absolute physical

standards, or standards traceable to the National Institute of Standards and Technology (NIST).

3.4 **Terahertz Time-Domain Spectroscopy (THz-TDS)**

Sample thickness was determined using a calibrated OriginCal caliper. A Teraview TPS 3000 (Teraview, Cambridge, UK) depicted in Figure 2 were used for THz-TDS measurements. THz spectra was collected from 0.2 to 1.4 THz under ambient conditions in transmission mode. Initial reference spectra were collected before sample data collection in pure nitrogen. Incident THz radiation energy was produced using a mode-locked Ti:Sapphire laser with a 800nm central wavelength, pulse duration of 100 fs, and a repetition rate of 80MHz: the incident THz pulse was divided into a pump and probe detection beams. The pump beam utilizes initial THz radiation, with the probe beam from the THz beam splitter in Figure 2 operating with a GaAs semiconductor detector. The optical and dielectric properties were collected in transmission mode, depicted in the bottom of Figure 2, then calculated by comparing the reference and sample time delay of the THz pulse with the inherent thickness of the sample. Collection of the THz spectrum is based on the ratio of the terahertz electric field strength transmission in equation 2.

$$\left(\frac{E_s}{E_r}\right) = T(n)\exp\left(-\frac{\alpha d}{2} + \frac{in\omega d}{c_0}\right) \tag{2}$$

Where the intensity before the sample is E_r and intensity after the sample is E_s, which gives the material characteristics. The quantity d is the sample thickness, ω the angular frequency of radiation, c_0 speed of light in a vacuum, and $T(n)$ the Fresnel reflection loss at sample surface. Measurement of the electric field strength ratio leads to dispersion collection of the refractive index n and the absorption coefficient α.

Refractive index measurements are collected by the relative phases of the sample φ_{SO} and reference φ_{RO} terahertz pulses from the imaginary part of the time-frequency Fourier transformation given by equation 3.

$$nd = \frac{c}{\omega}(\varphi_{SO} - \varphi_{RO}) \tag{3}$$

Absorption coefficients in the terahertz region were obtained from the electric field comparison between the sample and reference given by equation 4.

$$\alpha d = -20\log[\frac{(A_{SO}/A_{RO})}{T(n)}] \quad (4)$$

The coefficients A_{SO} and A_{RO} were obtained from the real part of the fast Fourier transform. Terahertz data analysis employed raw Boxcar apodization with signal processing through TPS software.

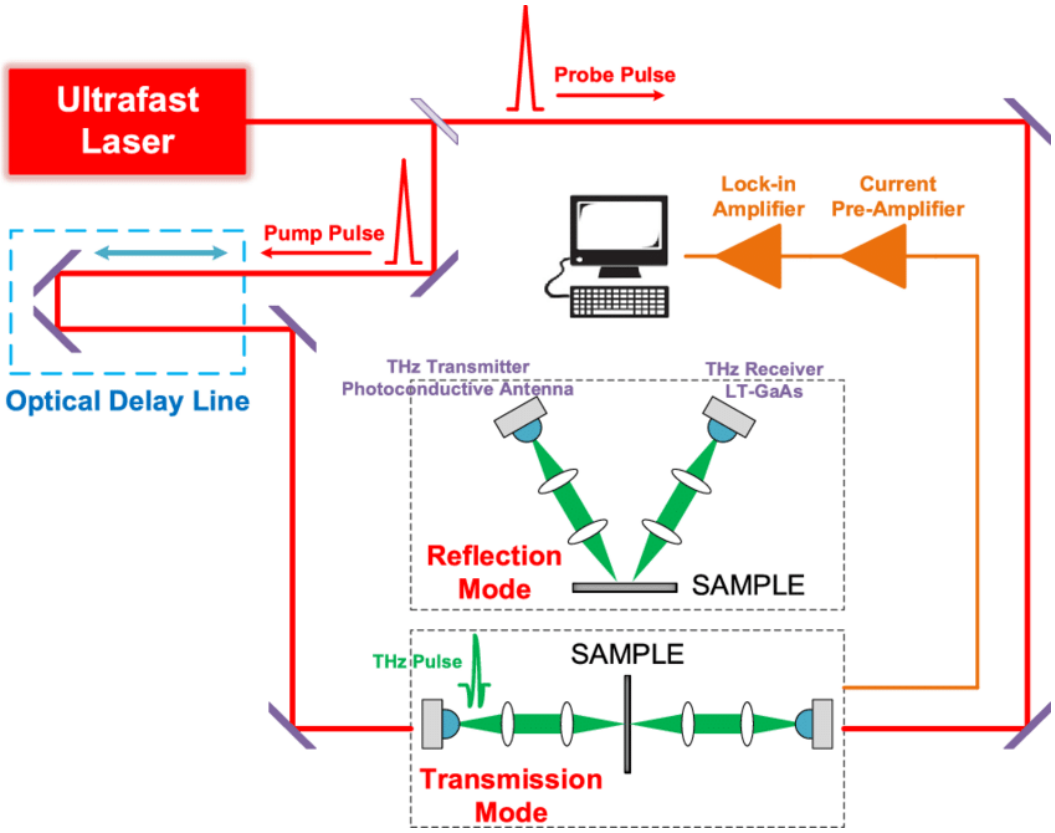

Figure 2. Teraview TPS300 schematic diagram[56]

3.5 **Density Measurements**

Density quantities were determined using a 33340 Mettler Density Determination Kit (Mettler Instrumente, Greifensee, Switzerland) and a Mettler AE 100 scale Mettler Instrumente, Greifensee, Switzerland) using the Archimedes method at 12°C using ultra-pure ethanol.

3.6 **Femtosecond Laser irradiation**

Laser irradiation of the SAL-glasses were conducted using a Femtoscoure scientific XL 500 femtosecond laser (FEMTOLASERS, Fernkorngasse, Vienna) in Figure 3. Pulse energy was estimated to be 500nJ with a central wavelength of 800nm with a repetition rate of 5.1MHz resulting in a projected pulse duration of less than 50fs. Glass specimens were optically polished discs, where laser modification was focused at the surface of the glass and rastered in separated regions of 3mm diameter at a rate of 250µm/s and 150µm/s. Beam diameter was estimated to be in the range 2µm at the surface after transmission through the beam sampler and plano-convex lens in Figure 4. Step sizes of the translational stage were programmed move 5µm vertically after horizonal rastering of the given velocities. Average power readings before the sample were between 1.7-1.9W.

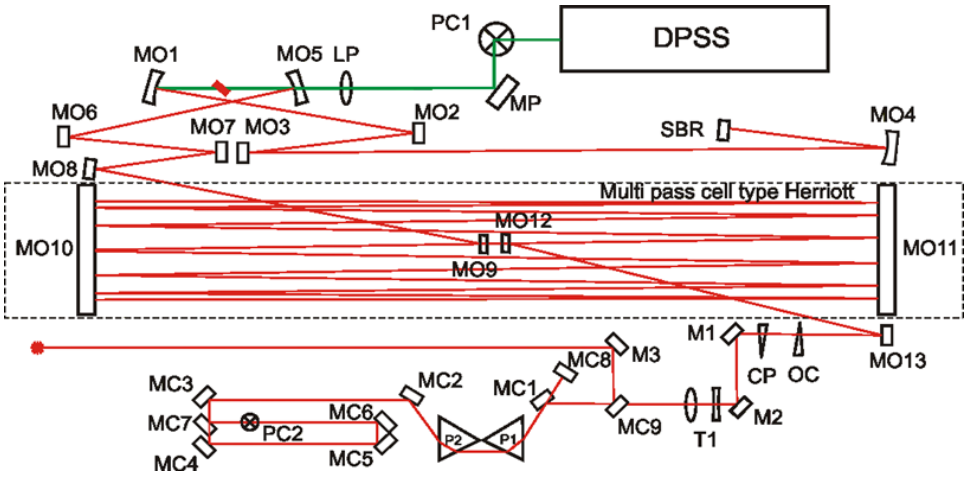

Figure 3. Femtoscoure XL-500 schematic diagram

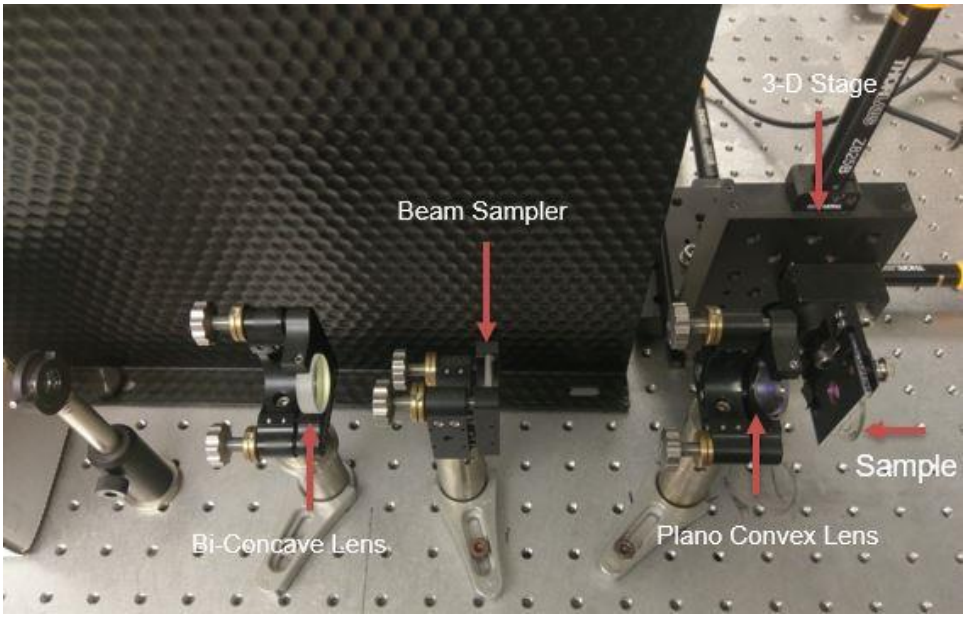

Figure 4. Femtosecond laser irradiation optics before sample

3.7 ^{27}Al MAS-NMR

^{27}Al MAS NMR data were collected using a commercial spectrometer and 3.2mm MAS NMR probe (Agilent DD2), in conjunction with a 16.4 T superconducting magnet. The resonance frequency of 27Al at this magnetic field was 182.34 MHz. Glass samples were powdered with an agate mortar and pestle, packed into 3.2mm outer diameter zirconia rotors, and then measured with sample spinning of 22 kHz. ^{27}Al MAS NMR spectra were acquired using radio-frequency pulses with a p/12 tip angle of 0.6 ms, a recycle delay of 4s and signal averaging of 800 transients. Data were processed without apodization and referenced to the shift of aqueous aluminum nitrate (0 ppm). Fitting of ^{27}Al MAS NMR data was performed with DMFIT[52], using the CzSimple function to account for distributions in quadrupolar coupling constant for each of the aluminum resonances. Several of the glass compositions were shown to contain a small amount of background signal from the zirconia rotor, which was confirmed by measuring the 27Al MAS NMR data for an empty rotor. This weak signal, centered around 1.5 ppm, was included in the peak fitting, but not used in determining peak areas and Al coordination numbers.

3.8 **Thermal treatment and X-ray diffraction (XRD)**

Heat treatment were preformed on bulk SAL glasses. Samples were reheated from ambient conditions to 1060°C with 10°C/min ramp rate and held at the temperature for 4h and then cooled down back to ambient temperature at a rate of 5°C/min. X-ray diffraction was done using a D2 PHASER (Bruker, Madison, WI, USA) on the heat-treated specimens. The angle range collected was between 10 and 80 2θ positions with a step size of 0.030.

III. RESULTS AND DISCUSSION

1. Differential Scanning Calorimetry (DSC)

Glass transition temperatures of the SAL-glasses were estimated from the onset temperature of the endothermic slope in Figure 5. The range of the SAL glasses display a narrow glass transformation region between 871-884°C. Apparent decreasing trend in T_g seems to correlate with the increase of lanthanum content. With the increase of La_2O_3 the silica content is lowered, where the concentration of NBO increase from lanthanum may decrease the structural crosslinking framework in terms of 4-fold Si and Al network formers with modifier characteristics.

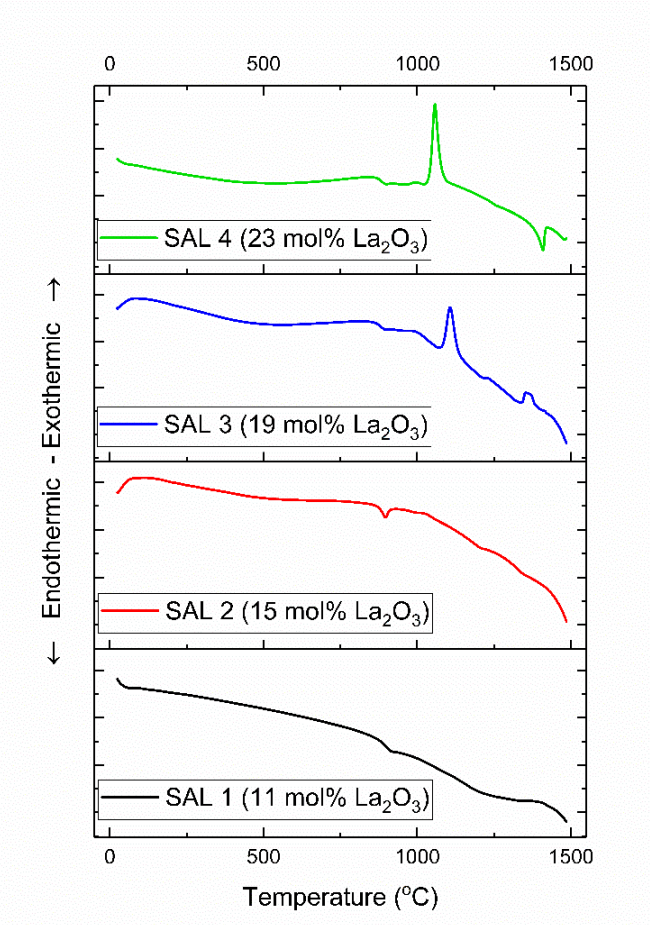

Figure 5. DSC thermal curves of SAL glasses

Table II - SAL Glass Transition Crystallization Temperatures

Sample	SAL1	SAL2	SAL3	SAL4
T_g(°C)	884	876	874	871
T_c(°C)	N/A	N/A	1108	1058

Lanthanum (La) addition shows an increase in aluminum coordination numbers, with the polymerized Al atom units increasing to 5 and 6-fold coordination. The Al-speciation is dependent on La-ions where it can possess a duality of glass formation characteristics. The La ions compensate the charged Al-species[53]. Al- speciation shows features of network forming or network modifier by octahedral configuration of the cation. The relatively high glass transition compared to similar works[19,30] may be evident of the large alumina content contribution to network forming. The narrow range of glass transitions temperatures might be due to the similar valency of cations of La and Al but the larger cation the increase of coordinate links can be formed and resulting in a slight decrease of networking cross linkages reported by Aronne et al[53]. Beyond the glass transition temperatures, the SAL glasses with higher La content show exothermic peaks indicative of devitrification, where the stability of the glass structure energy decreases with a higher tendency towards devitrification.

2. Ultraviolet-Visible (UV-Vis) Spectroscopy

Increase of the refractive index of the SAL glasses display the influence of polarizability from the La-cation additions in Figure 6. SAL glass sample refractive index dispersion The absorption edge from UV-Vis spectroscopy in the SAL glasses show a decreasing trend in the apparent bang gap energy as the La content increases in Figure 7. Band gap calculations from UV-Vis spectra. The shift in the absorption edge towards the visible spectrum is influenced by increasing La content which suggests conversion of the network oxygen to the non-bridging oxygen (NBO), where the larger concentration of SiO_2 tends to increase the energy of the absorption edge with increased Si-O linkages[54]. Band gap energy contribution of the silicate network could arise from the effect of La acting as

network modifier creating NBOs. The resulting decrease in the band gap has been correlated to the energy level transfer, which has been shown to decrease and attributed to the glass network disorder with the presence of lanthanum ions[55]. The relatively large band gap associated with the SAL-glass displays photoionization stability for significant nonlinear optical photon absorption with the addition of heavy La ions within the light aluminosilicate glass network.

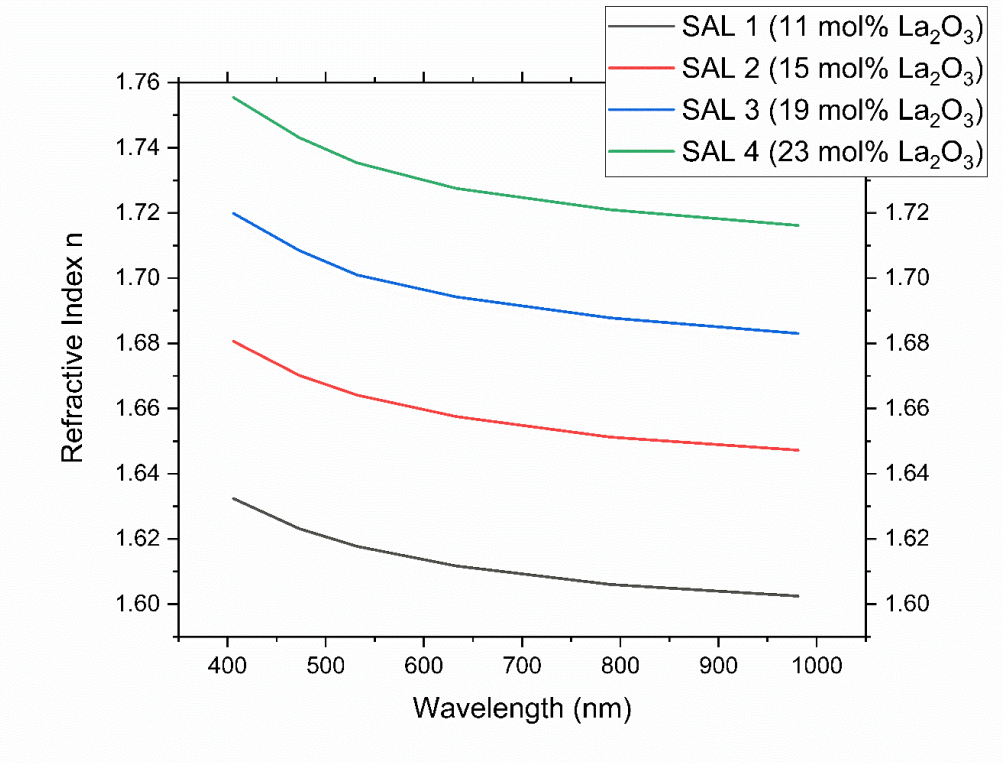

Figure 6. SAL glass sample refractive index dispersion

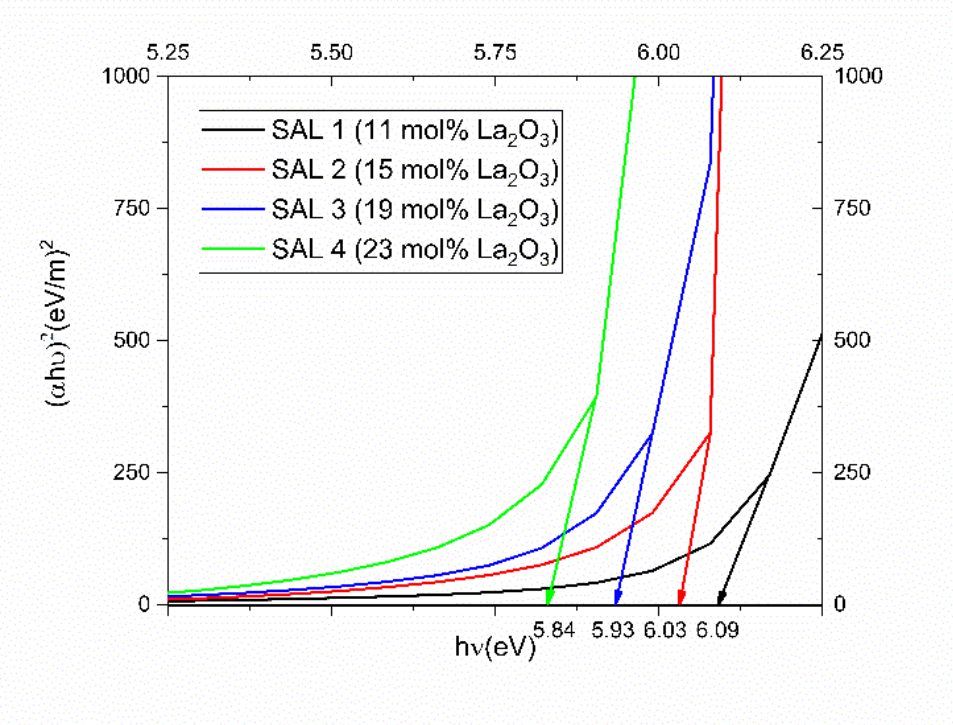

Figure 7. Band gap calculations from UV-Vis spectra

3. Polarizability and Refractivity

Refractive index correlations to the optical basicity by Duffy [21,26] utilized the molar polarizability. Specifically, for isotropic materials and disordered homogeneous dielectrics such as glasses, the molar polarizability (α_m) can be calculated form the Lorentz-Lorenz relationship with the molar volume (V_m) of a compound and its corresponding refractive index. Oxide based glasses have been associated to the optical basicity determined by the estimation of the average polarizability due to the oxygen contributions in the oxidation state of -2 charge[29,41]. Where the molar electronic polarizability can be calculated by the summation of individual cations and anions. The variability of the distortable state of oxygen ions needs to be considered and subtract the polarizability contribution of the cations within the substance. In order to calculate the oxygen influence, the value of the electron polarizability must be averaged by the total number of oxygens within the glass structure. The resulting influence gives the average oxygen polarizability $\alpha_{O^{-2}}$. The effective polarizability value represents the average state of the electron charge clouds of oxygen after they have participated in forming the glass structure[28]. The values can then be

indicative of the dipole electron response in terms of how ridged or floppy the distortable state is based on the magnitude of the oxygen polarizability.

The negative charge of oxygens available can be estimate on the degree of the charges relating to the absorption of the system. The optical basicity (Λ) value can is correlated to the degree of polarization based on the quantity of charges. Studies of the optical basicity of binary silicate oxide systems have been extended to oxidic glass systems with good agreement to calculate the optical basicity using the average state of polarization of the oxygen atom[23,35,60–62].

$$\Lambda = \frac{(3.133\alpha_{O^{-2}} - 2.868)^{1/2}}{1.567} - 0.362 \quad (5)$$

The values in

Table III shows the calculated values of polarizability from refractivity data of SAL

Glass Specimen	Density g/cm^3	Refractive Index @ 589nm	Molar Volume (cm^3)	Molar weight	Molar polarizability (Å^3)	Polarizability of Cations (Å^3)	Oxygen Polarizability $\alpha_{O^{-2}}$ (Å^3)	Optical Basicity Λ
SAL1	3.383	1.614	29.128	98.5284	4.025	32.434	1.588	0.564
SAL2	3.761	1.660	29.023	109.156	4.247	42.928	1.611	0.580
SAL3	4.070	1.697	29.432	119.784	4.495	53.422	1.643	0.602
SAL4	4.351	1.731	29.975	130.414	4.748	63.916	1.677	0.624

glasses. Figure 8 shows the accumulative polarizability and optical basicity of the SAL glasses. The linear increase observed may be attributed to the addition of lanthanum oxide content. The large degree of increasing the refractive index and can also be correlated to the increase of the density where the heavy lanthanum ions contribute to the bulk density. The oxygen influence from additions of lanthanum oxide are estimated with the optical basicity. The molar volume of the glasses do not show the additive linear increase with lanthanum concentration in the glasses. This is due to the rate of change of the density and

molecular weight. The increase of lanthanum content displayed a greater rate of change due to the molecular weight than the density when the silica content was lowered, leading to a possible opening of the glass network[56]. Oxygen packing density may decrease the molar volume causing an increase of the mass density of the SAL glasses.

Table III - Values of polarizability from refractivity data of SAL glasses

Glass Specimen	**Density** g/cm^3	**Refractive Index @ 589nm**	**Molar Volume** (cm^3)	**Molar weight**	**Molar polarizability** $(Å^3)$	**Polarizability of Cations** $(Å^3)$	**Oxygen Polarizability** $\alpha_{O^{-2}}$ $(Å^3)$	**Optical Basicity** Λ
SAL1	3.383	1.614	29.128	98.5284	4.025	32.434	1.588	0.564
SAL2	3.761	1.660	29.023	109.156	4.247	42.928	1.611	0.580
SAL3	4.070	1.697	29.432	119.784	4.495	53.422	1.643	0.602
SAL4	4.351	1.731	29.975	130.414	4.748	63.916	1.677	0.624

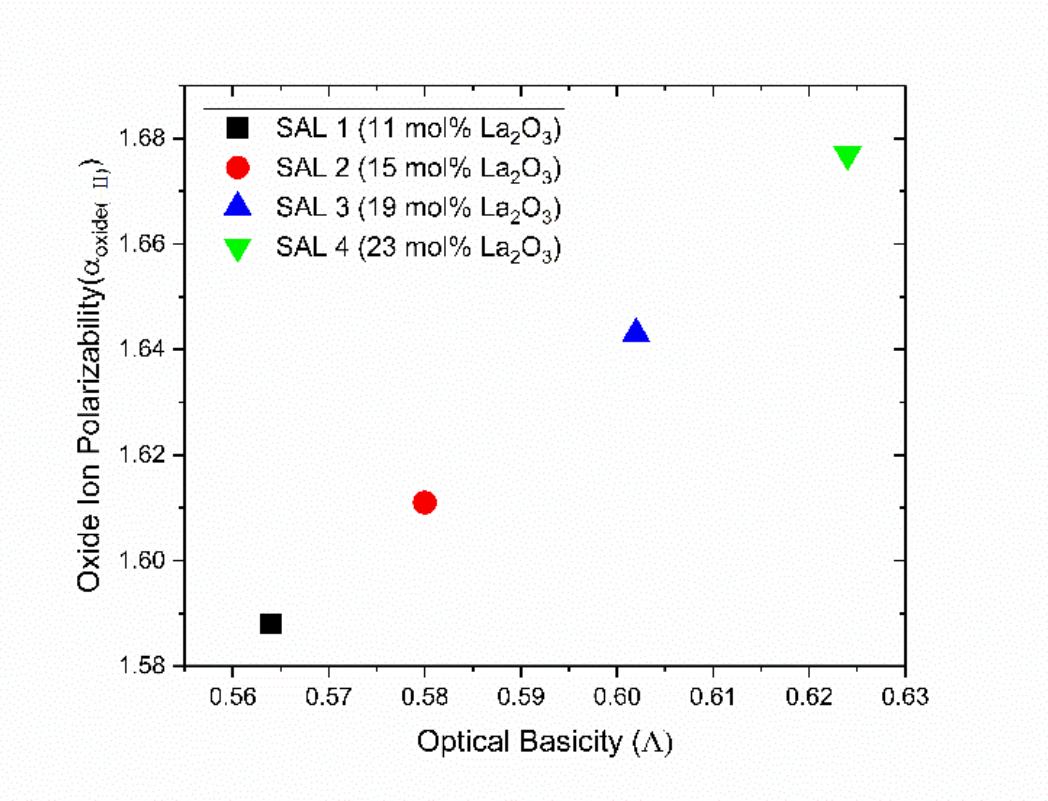

Figure 8. Accumulative oxide polarizability with optical basicity

The contributing influence can be estimated by the La content, which increases the density of the material with content. The electronic polarizability of the cations have been taken from references, which show that La ion has the highest electronic polarizability compared to silicon and aluminum[21,22]. Influence from lanthanum oxide is the increasing oxygen content since the cation contribution is removed from the molar polarizability. The optical basicity was calculated, assuming the Al-species were in 4-fold configuration. The Increase of the optical basicity displayed the ability of the oxide ions to donate electrons to the surround cation. The basicity results display the increasing negative charge on the oxygen atoms, which can be indicative of the increasing covalency in the cation-oxygen bonding[56].

However, the speciation of Al-species will polymerize in 5 and 6-fold with lanthanum content seen in ^{27}Al MAS-NMR data. The stereochemical change of the coordination number can be estimated by refractivity of aluminosilicate systems where the

Al-species can be regarded as less acidic with the decrease in optical basicity compared to SiO_2. The degree of acidity for the phases of alumina in coordination numbers can be described as the moderating parameter from polarizability. The moderating parameter used for Al coordination states have shown to differ with values ranging over 1.65-2.55 for the coordination of alumina[26]. Increases of the parameter indicate that there is an increase of acidity when incorporated with silica in aluminosilicates. Based on refractivity data for aluminosilicate systems the density and refractive index of $\alpha - Al_2O_3$ and $\gamma - Al_2O_3$ decrease with increasing coordination number. However, the slight increase in higher order Al-species will be drastically lower than the contribution of La_2O_3content as seen in the optical basicity and bulk refractive index data. The average oxygen contribution to the polarizability depends on the $[Al_2O_3]/([Al_2O_3] + [La_2O_3])$ concentration.

Figure 9 shows the overlap of the collected results in red superimposed on Naftaly and Miles work[45] from RI calculated with Cauchy dispersion equation. Where the increased trend in the data is due to the La affecting the glass structure and consequently the RIs. The polarizability relationship with RI from the Clausius-Mossotti equation can correlate the bond strength and configuration within the network.

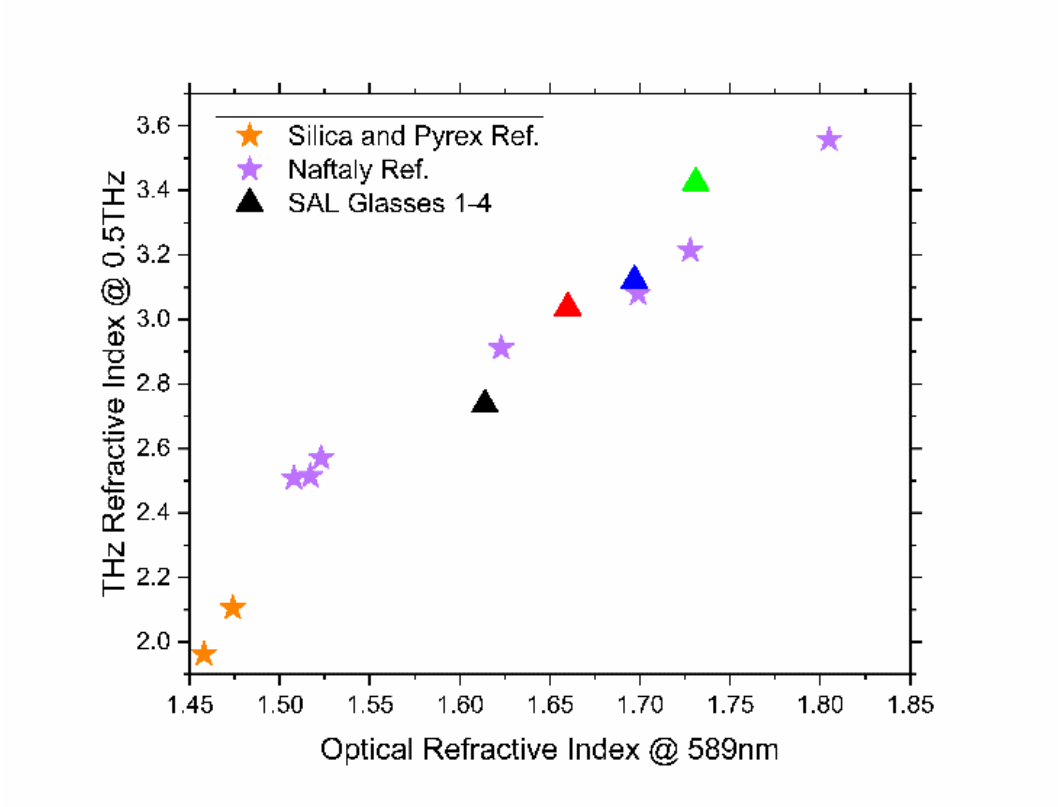

Figure 9. SAL glass series with Naftaly et. al THz-TDS and optical references[46]

The Thz and optical refractive index results display that as the La content increases the distribution of Al-species, increases of the NBOs within the glass can be detected coherently in the THz regime. An increase in the refractive index in THz regimes compared to the optical refractive index is increased due to the ionic polarizability which may lead to increased detection limit of the refractive index. Correlations between the refractive index and absorption coefficient against frequency allowed for experimental determination of the absorption parameters k and beta. Increasing the absorption parameter k from the Strom model[63] will scale with the refractive index.

Optical refractive index of the SAL glasses show an increasing tend with La content in Figure 10. The optical refractive index will be governed by the electron density and polarizability where the high field strength of lanthanum and the replacement of SiO_2 by Al_2O_3 will increase the polarizability by lowering the concentration of covalent bonding which will increase the formation of NBOs[57]. THz-TDS results of the refractive index has been shown to increase with the contribution of ionic polarizability, shown by the initial calculation of the optical basicity and the corresponding polarizability in Figure 8. The linear dependence can be extended to the THz frequency region, as with the optical refractive indices in Figure 10. The SAL glass systems from NMR results display a highly disordered framework where THz spectroscopy will be advantageous since the absorption will increase due to the polarizability[47]

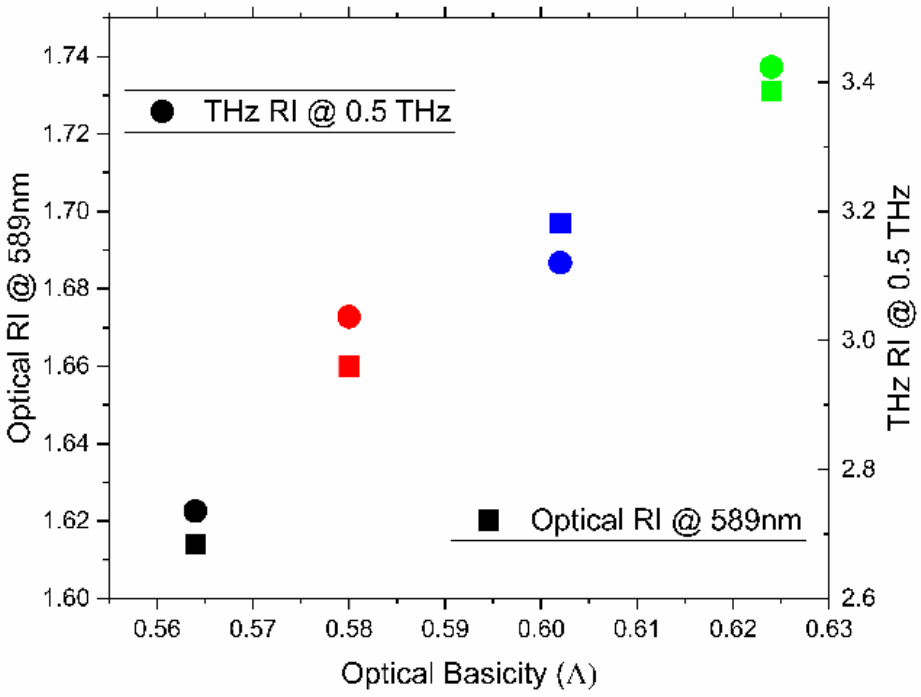

Figure 10. SAL glasses THz and optical basicity with oxygen polarizability

The linear correlation between the optical basicity and the refractive index in the optical region in Figure 8 show similar dependence between the terahertz regime in Figure 10. SAL glasses THz and optical basicity with oxygen polarizability. The estimation of the polarizability and optical basicity assignment of the silicate system can then be extended to the refractive indices in the terahertz regime, which also gives greater discernibility between minute differences compared to the optical regime.

4. ^{27}Al MAS-NMR

Figure 11 displays the ^{27}Al MAS-NMR chemical shift with three central transitions regions and asymmetrical shape indicative of aluminosilicate glasses. Noticeable shoulders occur in the 0- 25ppm range of shift in the spectra relating to the increase of Al-species polymerization increase with La additions. The chemical shift from 3QMAS-NMR deconvolution shows that the local coordination of Al-species is altered from the increase of La_2O_3. This may be caused by the positive trivalent La_2O_3, which acts as a charge

compensator on the negatively-charged Al(IV) species. Table IV shows an increase of Al(V) and Al(VI) polyhedra as the lanthanum content is increased sequentially with lowered SiO_2concentrations. Reports of the elastic moduli of SAL glasses show that La ions influence the Al-coordination species[15] with deviations of the elastic moduli predictions from the Makishima and Mackenzie model[58] which incur by the inclusions of higher coordinated Al species, where the model predicts a two-dimensional structure. Comparison to literature confirms from that the BO/NBO glass network decreases as well as depolymerization of the Al species. The ^{27}Al MAS-NMR shows that with increasing the La content the aluminum speciation tend to increase into 5 and 6-fold coordination shown in Figure 11and Table IV. Shift in the absorption edge towards longer wavelengths with increasing La content displays a possible conversion of BOs to NBOs which will lower the band gap energy. Since the conversion of Al-species from 4-fold decreases and the higher order coordination of 5 and 6-fold increase, the network of the aluminum species with high La content is saturated with sufficient oxygen anions to alter the network framework of the Al(IV) species to higher order species as well as increase the NBOs. Influence of the presence of five-fold Al-species have been reported by Stebbins et. al [36,59], which have contributions to the configuration evolutions in the species distribution with only nominal values. Coexistence of higher coordinated of penta- and hexa-coordinated Al-species have also shown to characterize amorphous alumina[60] which may also be incorporated thermally by being quenched within the structure allowing for deviations in bonding preferences between Al-species, with the high field strength of 6-coodinated lanthanum. The effects of the inclusions of the higher order species will alter the rigidity of the system with the contributions of higher coordinated Al-species.

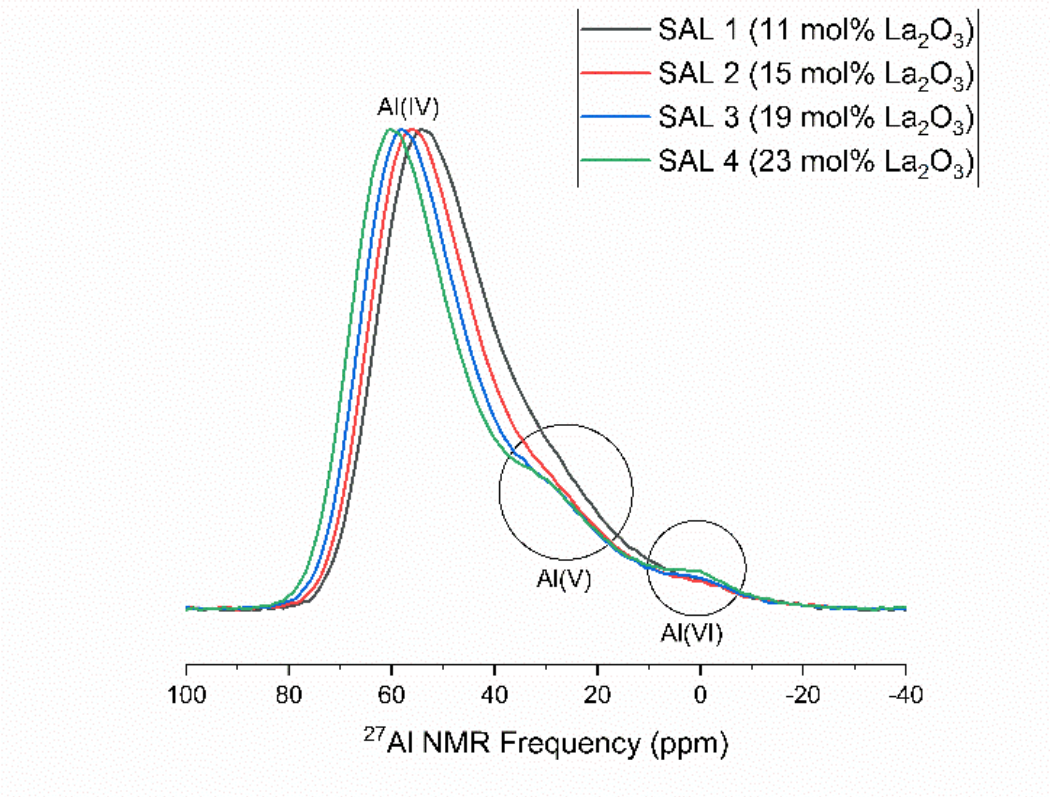

Figure 11. ^{27}Al MAS-NMR of untreated SAL glasses

Table IV - ^{27}Al 3QMAS-NMR

La_2O_3 (Mol %)	Al(IV)	Al(V)	Al(VI)
11	93.1	5.8	1.2
15	91.4	6.8	1.8
19	88.6	8.9	2.5
23	84.5	12.2	3.3

5. Femtosecond Laser Modification

Femtosecond laser modified regions of SAL-glasses were performed in two regions and one untreated pristine region. The laser irradiation parameters were kept constant with varying the rastering rate for a longer exposed duration between the two regions displayed in Figure 12. Optical refractive measurements in the optical regime measured via transmission prism coupler technique displayed a high degree of the standard deviation from multiple measurements in selected regions of the pristine and fs-laser modified regions. The discrepancy for the uncertainty values in the optical regime can be attributed to variations in the bulk material where possible low degrees of striae within the glass may have altered the optical refractive index. Measurements did show a trend for increasing the refractive index based on laser irradiation, but the uncertainty in modified regions limited the quantification for the change in the refractive index based on fs-laser irradiation.

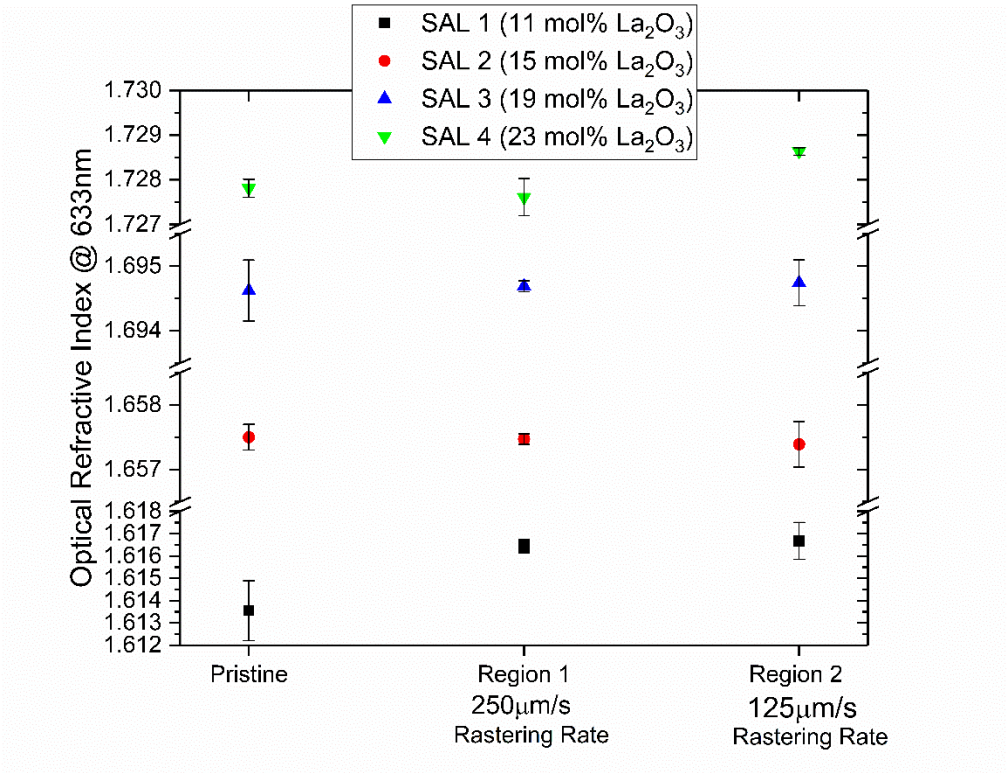

Figure 12. Optical refractive index measurements of fs-laser irradiated regions

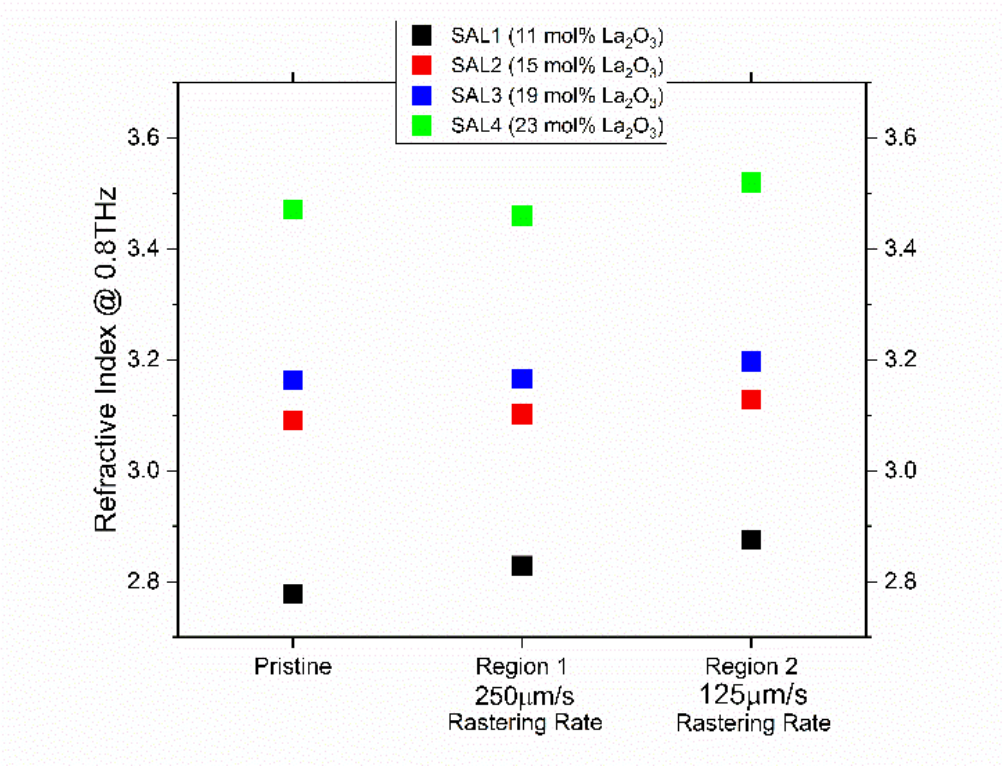

Figure 13. Terahertz refractive index based on irradiation to fs-laser

Upon fs-laser exposure, the refractive index in the THz regime increase for longer exposure times, as shown in Figure 13. Deviations in the change of the refractive index may be attributed to the fs-laser stability during exposure experiments, with multiple spectra recorded in the THz regime. The spectra displayed no change in the THz region of interest, with only deviations in higher Thz ranges due to back reflection oscillations. Refractive measurements in the THz have an inherent nature for increasing the magnitude of refractive index differences based on the sensitivity of oxygen polarizability contributed by the additions of network modifiers. Increased THz refractive indices compared to optical can also be attributed to the polarizability of polar dielectric properties from the contributions of both electronic and ionic polarizabilities. The enhancement of oxygen polarizability has been shown on the base SAL glasses systems, where the increase of La_2O_3can be attributed to creating non-bridging oxygens as well has increase the content of heavy La^{3+} cations. Concentration of alumina species depend on the content of lanthanum within in the system. However, upon irradiation the increase in the refractive index from THz data shows that the Al-species are altered based on femtosecond laser

irradiation supported by ^{27}Al-MAS NMR data shown in Table V. Figure 14 shows the increase in 5 and 6-fold Al species in Table V. For fs-laser modified regions, the increased exposure trend displays a further network deformation of increased distribution of Al-species. The energy densities increase the structural reconfiguration of the network forming Al-tetrahedra into 5 and 6-fold coordination. The charge balancing influence of the La cations have been shown to avoid heterogeneous clustering of rare earth ions by fluorescence line broadening effect[61]. Influence from the fs-laser may induce the creation of non-bridging oxygens or the polarizability of the locally modified regions resulting in the increase of the refractive indices shown in Figure 13 of the THz-TDS data.

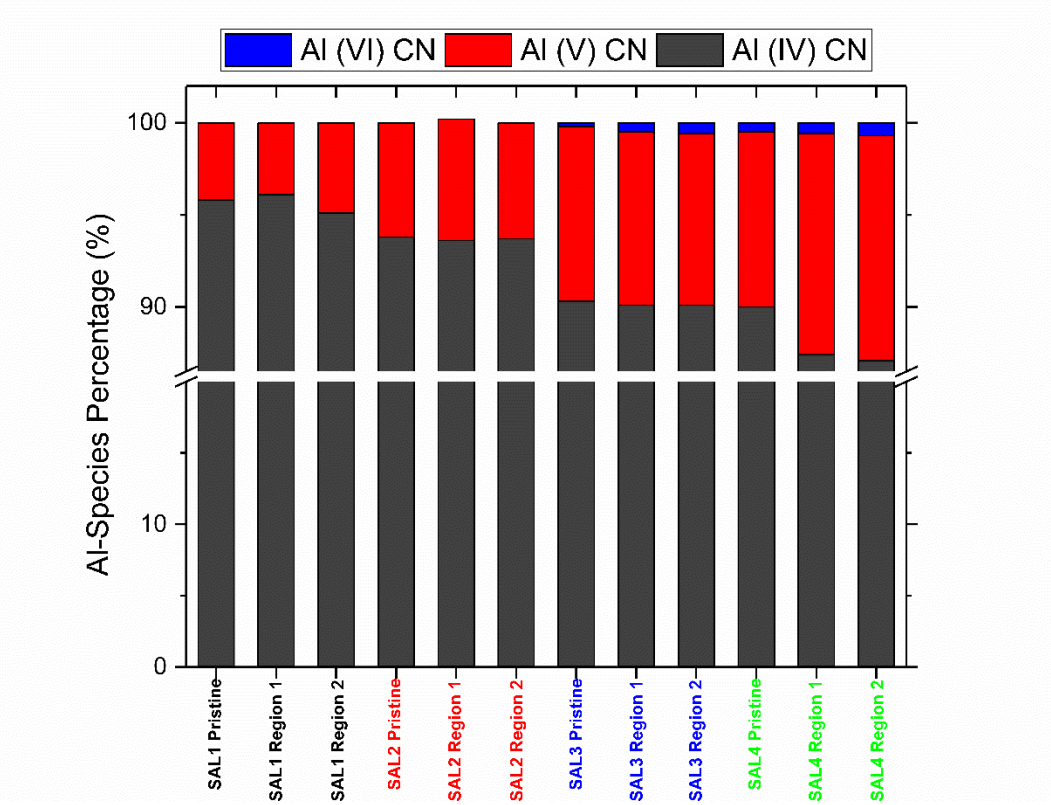

Figure 14. ^{27}Al MAS-NMR of Fs-Laser Modified Regions

The refractive index increases for the bulk glasses with increase in polymerization of the network of Al-species. The increased trend of 5 and 6-fold Al-species are seen from further ^{27}Al-MAS NMR where the irradiation may increase the coordination of alumina species within the same compositions. The local irradiation of the regions in the bulk glass show increase the Al-coordination distribution units in the structural connectivity of the glasses. Local density of the irradiated regions may be altered from the consistent base chemical composition. However, local disorder of the connectivity of Al-species differed from the pristine regions to the modified regions in Table V. Fitting parameters of the NMR spectra resulted in the estimation of Al-species on the corresponding chemical shift. Depolymerization was shown to be evident based on composition shown in the bulk glasses in Figure 11. Local modification by fs-laser irradiation may influence the local structure, e.g., the coordination of the Al-species from the NMR study. The increase in the higher order Al-species upon irradiation can possibly be attributed to the configuration effects of these species contributing to relaxation, and an increased density in the regions.

Table V - Summary of ^{27}Al MAS NMR data of fs-laser modified regions

Specimen	**Al(IV)**	**Al(V)**	**Al(VI)**
SAL1 Pristine	95.8	4.2	0
SAL1 Region 1	96.1	3.9	0
SAL1 Region 2	95.1	4.9	0
SAL2 Pristine	93.8	6.2	0
SAL2 Region 1	93.6	6.6	0
SAL2 Region 2	93.7	6.3	0
SAL3 Pristine	90.3	9.5	0.2
SAL3 Region 1	90.1	9.4	0.5
SAL3 Region 2	90.1	9.3	0.6
SAL4 Pristine	90	9.5	0.5
SAL4 Region 1	87.4	12	0.6
SAL4 Region 2	87.1	12.2	0.7

6. Terahertz Time-Domain Spectroscopy (THz-TDS)

Optical Basicity of glass has been determined by estimating the average oxygen polarizability based on the constituents of the lanthanum aluminosilicate glass system. The model developed by Strom et al[62], for the explanation of the absorption coefficients in far-infrared absorption of amorphous materials is shown as:

$$n(\nu)\alpha(\nu) = K_0(h\nu)^{\beta} \quad (6)$$

Considering the magnitude of the far infrared conductivity and absorption by Strom, the power-law relation in Equation 6 is used for quantitatively determining the exponent β and coefficient K based on the structure of an amorphous material. The coefficient K, based on the absorption coefficient and refractive index dispersion, should scale with the increase of the density of charge fluctuations in the material. Based on the composition of the SAL-glasses, the coefficient K should increase with the refractive index. Naftaly[43] illustrates an increasing trend with the fraction of ionic network modifiers in the glass and also states the coefficient indicates an inverse relation to the bonding strength of the glass, based on alkali additions[42]. Deviations from the Strom model[62], where larger K-values is experimentally determined, suggest that the enhanced coupling can be attributed to the type of ionic character of the alkali inclusion[45]. Strom et. al[62] describe the observed far-IR absorption to optical radiation with the disorder induced interaction of the lattice excitations of the amorphous solid. Figure 15 displays the increasing trend from the predictive optical basicity of the oxygen donor power contributing to the polarizability.

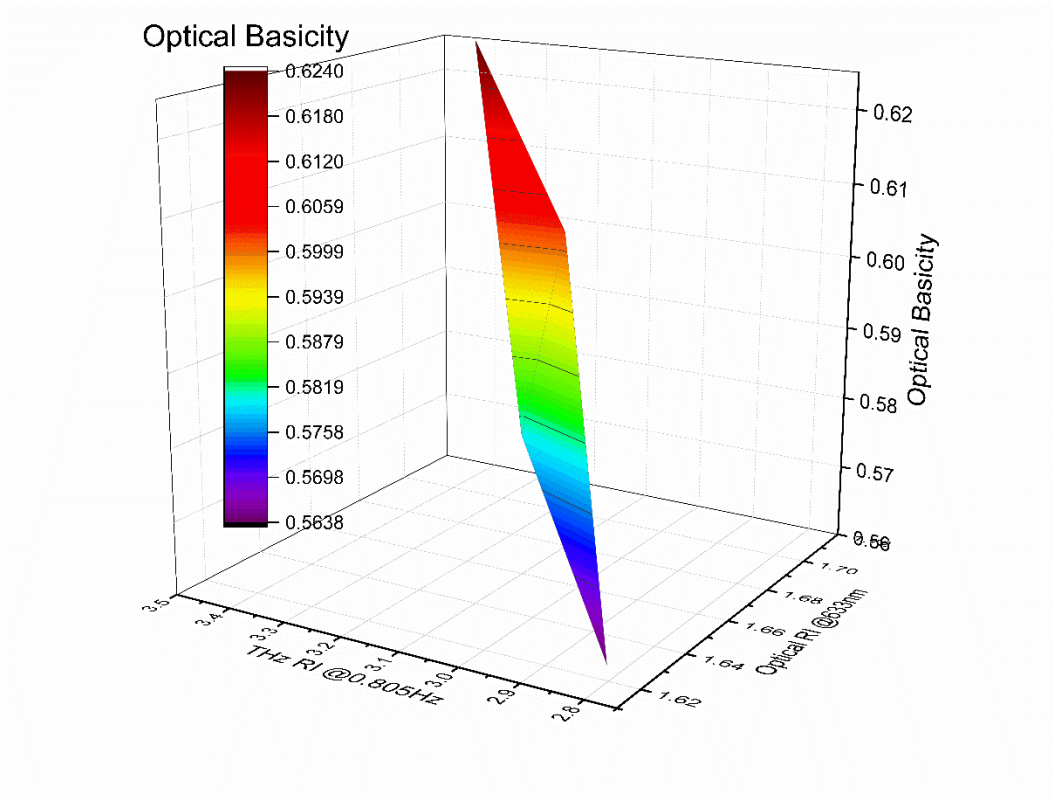

Figure 15. Refractive indices of optical and THz regimes to optical basicity

The linear correlation of optical basicity and THz-TDS refractive indices of the SAL-glasses show that it is possible to utilize the predictive power of optical basicity to extend to the THz region with greater discernibility than the optical regime. The lanthanum oxide additions affects the structural connectivity and evolution of the depolymerized Al-species with lanthanum content. The influence of the lanthanum alters the Al-species in the glass structural motifs converting the network forming tetrahedral species to possible edge and face sharing for intermediate characteristics of Al(V) and Al(VI). Density measurements also show the sequential increase for heavy lanthanum additions, which contribute to the increase of polarizability correlated to the refractive index. However, the visible refractive indices show a more pronounced error deviations from possible striae effects on the RI measurements. However, fs-laser and optical measurements were conducted in qualitative pristine regions by optical inspection. Refractive indices in the THz regime data show a larger differentiation in the RI based on the THz frequency

detection of the charge fluctuations, as shown in Figure 16. THz refractive index and absorption coefficient dispersion with the change in the fs-modified regions.

The optical error calculations were based of multiple prism couple measurements in the same rastered regions of each glasses recorded six times. Table VI shows the larger noticeable differences in the THz frequencies of the refractive index. Multiple THz-TDS measurements were conducted with each spectrum displaying identical spectra, with only higher THz variations above 1THz with possible back reflection contributions from the sample thickness. THz-TDS analysis was done with compiled data sets of three measurements in the same glass specimen regions.

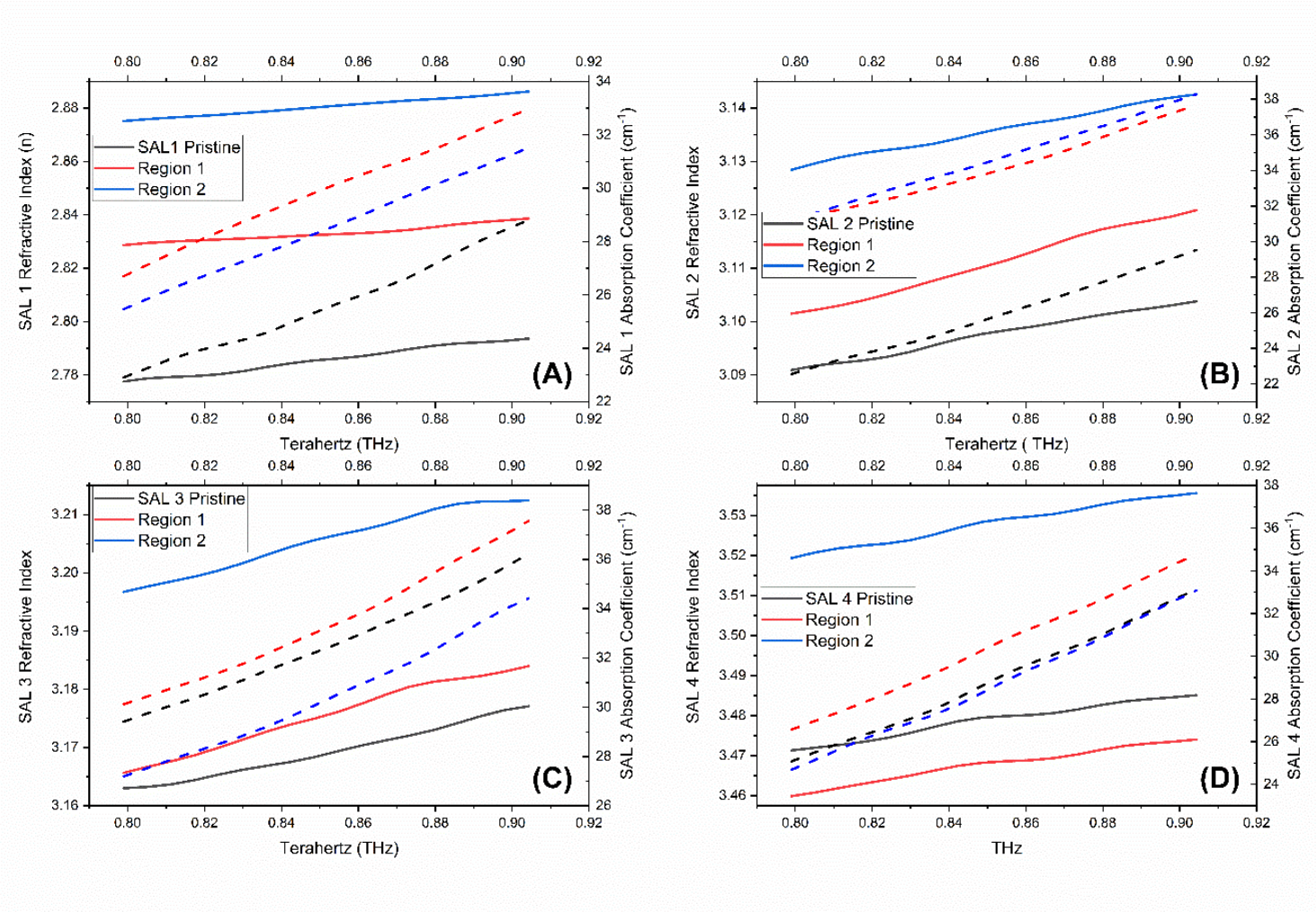

Figure 16. THz refractive index and absorption coefficient dispersion

Table VI - Fs-laser modified regions change in optical refractive index

Fs-Modified Region	**SAL 1 @633nm**	**Error**	**SAL 2 @633nm**	**Error**	**SAL 3 @633nm**	**Error**	**SAL 4 @633nm**	**Error**
Pristine n	1.6136	0.0013	1.6575	0.0002	1.6946	0.0005	1.7278	0.0002
Region 1 Δn	0.0029	0.0014	0.0000	0.0002	0.0001	0.0005	-0.0002	0.0005
Region 2 Δn	0.0031	0.0016	-0.0001	0.0004	0.0001	0.0006	0.0008	0.0002

Table VII - Fs-laser modified regions change in THz refractive index

Fs-Modified Region	**SAL 1 @0.805THz**	**SAL 2 @0.805THz**	**SAL 3 @0.805THz**	**SAL 4 @0.805THz**
Pristine n	2.7776	3.0909	3.1630	3.4713
Region 1 Δn	0.0511	0.0106	0.0026	-0.0114
Region 2 Δn	0.0975	0.0375	0.0337	0.0481

The absorption parameters show large increase based on high refractive index of the SAL glasses. Using the Strom model[62], the absorption parameter from THz-TDS method do not display a linear trend for the pristine or modified regions of the glasses. In comparison to works done by Naftaly[43], the increase of the K_0-value was estimated based on alkali modifier content compared to fused silica and Pyrex. Additions of REEs within the glass system show a similar trend with the increase of oxygens and cation field strength. The alumina coordination number estimates from NMR data show the trend for increased disorder of the linkages of the Al-species.

The THz range of investigation also limited the fitting of the parameter for a good estimation due to the narrower range of THz frequencies based on the noise difference from the sample thickness due to back reflections within THz-TDS. The structural order framework of REEs must also be taken into account, where the SAL-glasses may lack structure beyond the short-range view with a wide distribution of covalent bonding between specific species and bridging oxygens with possible tri-clustering. Addition of lanthanum may also act as a network modifier when of 25mol% of La_2O_3 is reached, where the formation of coordinate links overcomes the decrease of cross links. However, x-ray photoelectron spectroscopy (XPS) preliminary results displayed lanthanum consistency among each sample with noticeable f-f splitting. O1s high resolution spectra showed variances in broad peaks for indistinguishable and arbitrary deconvolution methods in estimating nominal binding energy differences. The polymerization of the glass matrix of tetrahedrally coordinated species contribute to the differences in THz measurements where the modified regions of equivalent chemical base compositions displayed a strong trend and correlation to the THz refractive indices.

Laser irradiation of each sample was accomplished with rastering regions with specific step-size for single mode irradiation. Power output differences of the laser varied to about 10% of total output power during rastering modes. Fluctuations in the power output may also vary the total power density of fs-laser irradiation. Thermal effects upon irradiation of the glasses may also be a factor for variations in the refractive indices, which will require further examination of the heat influence. However, no visual or microstructural (SEM) differences were found in the modified regions. Presence of the increased percentages of higher coordinated Al-species may be influenced by the power

density but the reconfiguration remains to be determined by the thermal influence of fs-modification.

7. X-Ray Diffraction (XRD)

XRD analysis of SAL specimens were generally amorphous in nature. However, heat treated samples shown in DSC results in Figure 5 show an increased tendency to devitrify with higher La_2O_3 content. Further XRD analysis of the heat-treated specimens displayed crystallization in well-defined peaks from XRD, shown in Figure 17. The Fitting of the spectral regions displayed an aluminum lanthanum silicate preference with higher lanthanum content specimens exhibiting similar Liottite crystal structure and unresolved aluminum silicate upon crystallization. Further XRD analysis was unable to identify the patterns with low degree FOMs using the Powder Diffraction File database.

SAL samples did visually show opaqueness a preference for surface devitrification and phase separation, which was evident in the lower lanthanum content glasses with noticeable phase separation. Surface crystallization may be attributed to the Al/Si ratio in composition series, where the crystal growth can be accounted for as a result of reduction the glass viscosity[32]. The lower viscosity in the SAL-species can be correlated to the diffusion rate for a Al/Si rich phase. The tendency for devitrification in the glass show that the structural ordering has a lower configurational energy requirement in the higher lanthanum content glasses, where the low La_2O_3 content glass displayed an amorphous character attributed to a non-equilibrium state. The coordination change based on composition shows the predominate structure forms in the SAL-glass with higher lanthanum content. The low lanthanum content glasses, SAL1 and SAL2 visually exhibited surface crystallization but did not fully crystalize internally of the pristine glass disk specimens. Devitrification appeared to be predominate in higher lanthanum content specimens, which may explain the preferential bonding of lanthanum to Al sites and possible isoelectronic preferences of the glass matrix formers of tetrahedral linkages. Partial crystallization and phase separation in SAL1 and 2 h compared to SAL 3 and 4 which tend to crystalize by means of structural reordering of Al-species and the probable electronic bonding difference.

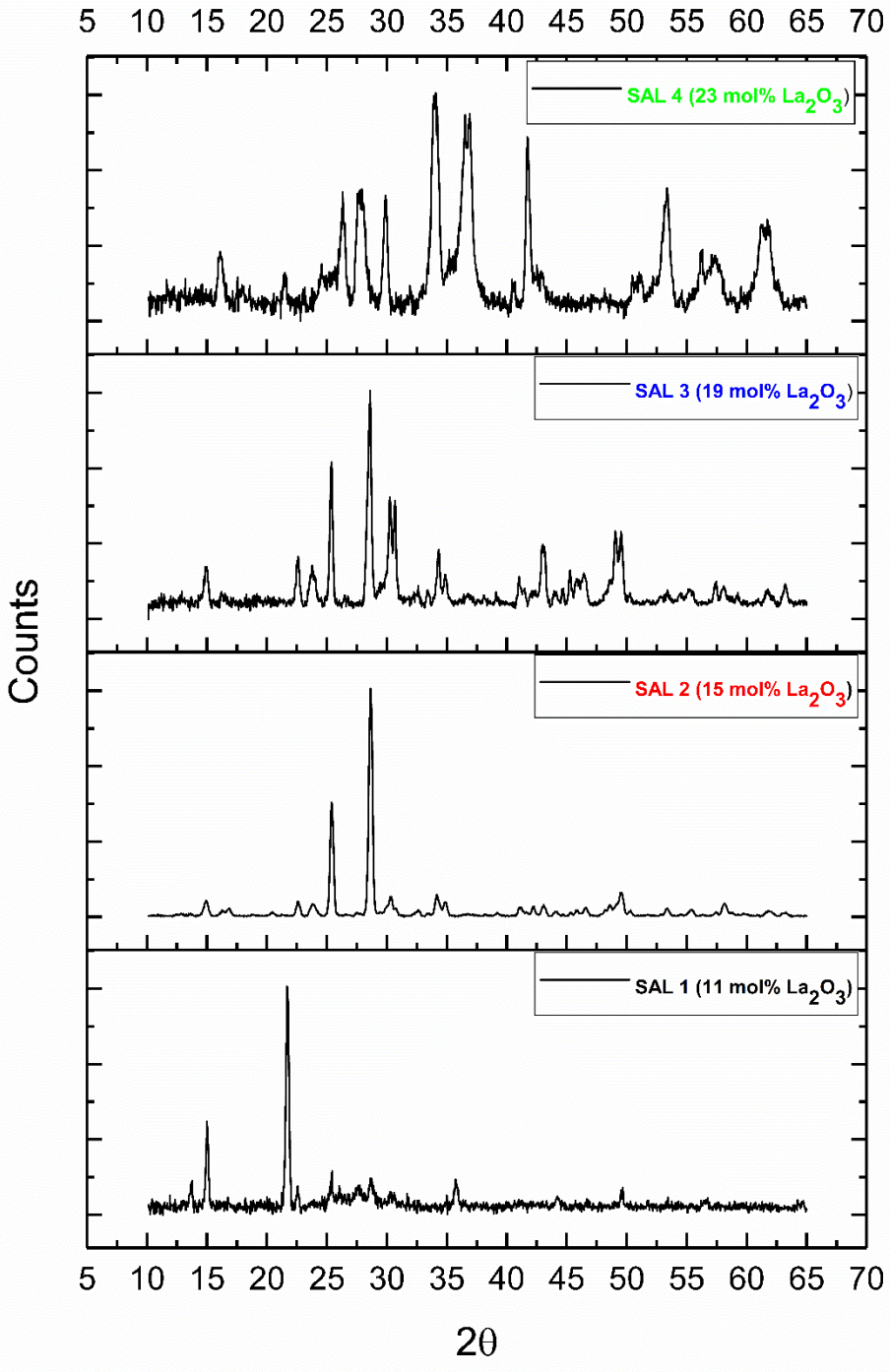

Figure 17. XRD of Heat treated SAL bulk glasses

IV. SUMMARY AND CONCLUSIONS

Laser-induced increasing density and visible refractive index with lanthanum content in SAL glasses is attributed to the heavy metal inclusions and increased polarizability. The ^{27}Al MAS-NMR results show that the increase in Al-species is due to high coordination numbers, reducing the network forming contributions of Al_2O_3. Upon fs-laser irradiation, the Al-species show a similar trend with increased irradiation in two laser-irradiated regions with a pronounced increase in THz refractive index, compared to the minute differences in the visible region. Further differentiation in the visible and THz frequencies show the increase spectral detection range for the refractive indices

V. FUTURE WORK

The main objective of this investigation was to determine the induced refractive index response of lanthanum aluminosilicate glass under femtosecond laser irradiation. The subtle alteration of the optical refractive index and modified laser volume posse the challenge of unique sample preparation. Further investigation would be of uniform sample thickness with a high degree of homogeneity. Altering rastering rates of the laser with varied repetition rate will be of interest to investigate the thermal effects from laser modification. Numerical aperture lenses before the sample to adjust the interaction volume should also be considered. Structural investigations would benefit from additional ^{29}Si and ^{17}O to determine local structure alterations of modified regions with respect to Si and O. Electron paramagnetic resonance (EPR) could provide insights on defect sites in these glasses from free oxygens or electron hole centers. Investigation with neutron diffraction may also benefit to determine the radial distribution function of the glasses. Fluorescence lifetime measurements will determine if there is any clustering effects.

VI. REFERENCES

1. L. G. Hwa, T. H. Lee, and S. P. Szu, "Elastic Properties of Lanthanum Aluminosilicate Glasses," *Mater. Res. Bull.*, **39** [1] 33-40 (2004).

2. S. Tanabe, K. Hirao, and N. Soga, "Elastic Properties and Molar Volume of Rare-Earth Aluminosilicate Glasses," *J. Am. Ceram. Soc.*, **75** [3] 503-6 (1992).

3. J. T. Kohli and J. E. Shelby, "Formation and Properties of Rare Earth Aluminosilicate Glasses," *Phys. Chem. Glasses*, **32** [2] 67-71 (1991).

4. J. Qiu, K. Miura, H. Inouye, Y. Kondo, T. Mitsuyu, and K. Hirao, "Femtosecond Laser-Induced Three-Dimensional Bright and Long-Lasting Phosphorescence inside Calcium Aluminosilicate Glasses Doped with Rare Earth Ions," *Appl. Phys. Lett.*, **73** [13] 1763-5 (1998).

5. A. Herrmann and C. Rüssel, "New Aluminosilicate Glasses as High-Power Laser Materials," *Int. J. Appl. Glass Sci.*, **6** [3] 210-9 (2015).

6. D. Litzkendorf, S. Grimm, K. Schuster, J. Kobelke, A. Schwuchow, A. Ludwig, J. Kirchhof, M. Leich, S. Jetschke, J. Dellith, J.-L. Auguste, and G. Humbert, "Study of Lanthanum Aluminum Silicate Glasses for Passive and Active Optical Fibers," *Int. J. Appl. Glass Sci.*, **3** [4] 321-31 (2012).

7. T. Minh Hau, X. Yu, D. Zhou, Z. Song, Z. Yang, R. Wang, and J. Qiu, "Super Broadband near-Infrared Emission and Energy Transfer in Bi–Er Co-Doped Lanthanum Aluminosilicate Glasses," *Opt. Mater.*, **35** [3] 487-90 (2013).

8. M. Naftaly and R. E. Miles, "Terahertz Time-Domain Spectroscopy for Material Characterization," *Proc. IEEE*, **95** [8] 1658-65 (2007).

9. M. S. Ahsan, R. S. Rafi, I.-B. Sohn, H.-K. Choi, and M. S. Lee, "Characterization of Femtosecond Laser Filamentation in Soda-Lime Glass," *2015 International Conference on Electrical Engineering and Information Communication Technology (ICEEICT)*, IEEE, New York 2015.

10. T. Toney Fernandez, P. Haro-Gonzalez, B. Sotillo, M. Hernandez, D. Jaque, P. Fernandez, C. Domingo, J. Siegel, and J. Solis, "Ion Migration Assisted Inscription of High Refractive Index Contrast Waveguides by Femtosecond Laser Pulses in Phosphate Glass," *Opt. Lett.*, **38** [24] 5248-51 (2013).

11. J. Solis, T. Teddy Fernandez, J. Hoyo, J. Siegel, and P. Zarate, "Femtosecond-Laser-Induced Compositional Changes for High-Performance Photonics,"; 1-4, *SPIE Newsroom*, Bellingham, WA, 2015.

12. S. M. Eaton, M. L. Ng, R. Osellame, and P. R. Herman, "High Refractive Index Contrast in Fused Silica Waveguides by Tightly Focused, High-Repetition Rate Femtosecond Laser" *J. Non-Cryst. Solids*, **357** [11-13] 2387-91 (2011).

13. C. B. Schaffer, A. Brodeur, and E. Mazur, "Laser-Induced Breakdown and Damage in Bulk Transparent Materials Induced by Tightly Focused Femtosecond Laser Pulses" *Meas. Sci. Technol*., **12** [11] 1784-94 (2001).

14. M. Hughes, W. Yang, and D. Hewak, "Fabrication and Characterization of Femtosecond Laser Written Waveguides in Chalcogenide Glass, *Appl. Phys. Lett.* **90** [13] 1311131-13113-3 (2007)

15. J. E. Shelby and J. T. Kohli, "Rare-Earth Aluminosilicate Glasses," *J. Am. Ceram. Soc*., **73** [1] 39-42 (1990).

16. A. Rosenflanz, M. Frey, B. Endres, T. Anderson, E. Richards, and C. Schardt, "Bulk Glasses and Ultrahard Nanoceramics Based on Alumina and Rare-Earth Oxides," *Nature*, **430** [7001] 761-4 (2004).

17. A. J. G. Ellison and P. C. Hess, "Solution Properties of Rare Earth Elements in Silicate Melts: Inferences from Immiscible Liquids," *Geochim. Cosmochim. Acta*, **53** [8] 1965-74 (1989)

18. V. R. Bhardwaj, E. Simova, P. B. Corkum, D. M. Rayner, C. Hnatovsky, R. S. Taylor, B. Schreder, M. Kluge, and J. Zimmer, "Femtosecond Laser-Induced Refractive Index Modification in Multicomponent Glasses," *J. Appl. Phys,* **97** [8] 083102-083102-9 (2005).

19. S. Iftekhar, J. Grins, and M. Edén, "Composition–Property Relationships of the La_2O_3- Al_2O_3-SiO_2Glass System," *J. Non-Cryst. Solids*, **356** [20] 1043-8 (2010).

20. B. Stevensson and M. Edén, "Structural Rationalization of the Microhardness Trends of Rare-Earth Aluminosilicate Glasses: Interplay between the RE^{3+} Field-Strength and the Aluminum Coordinations," *J. Non-Cryst. Solids*, **378** [1] 163-7 (2013).

21. J. A. Duffy, "Polarisability and Polarising Power of Rare Earth Ions in Glass: An Optical Basicity Assessment," *Phys. Chem. Glasses*, **46** [1] 1-6 (2005)

22. X. Zhao, X. Wang, H. Lin, and Z. Wang, "Electronic Polarizability and Optical Basicity of Lanthanide Oxides," *Physica B,* **392** [1] 132-6 (2007).

23. V. Dimitrov and T. Komatsu, "Classification of Oxide Glasses: A Polarizability Approach," *J. Solid State Chem.,* **178** [3] 831-46 (2005).

24. J. A. Duffy, "A Review of Optical Basicity and Its Applications to Oxidic Systems," *Geochim. Cosmochim. Acta*, **57** [16] 3961-70 (1993).

25. V. Dimitrov and S. Sakka, "Electronic Oxide Polarizability and Optical Basicity of Simple Oxides. I," *J. Appl. Phys,* **79** [3] 1736-40 (1996).

26. J. A. Duffy, "Optical Basicity of Aluminosilicate Glasses," *Phys. Chem. Glasses* **43** [6] 388-92 (2003).

27. V. Dimitrov and T. Komatsu, "Electronic Polarizability, Optical Basicity and Non-Linear Optical Properties of Oxide Glasses," *J. Non-Cryst. Solids*, **249** [2] 160-79 (1999).

28. V. Dimitrov and T. Komatsu, "An Interpretation of Optical Properties of Oxides and Oxide Glasses in Terms of the Electronic Ion Polarizability and Average Single Bond Strength," *J. Univ. Chem. Technol. Metall.*, **43** [3] 219-50 (2010).

29. X. Zhao, X. Wang, H. Lin, and Z. Wang, "Average Electronegativity, Electronic Polarizability and Optical Basicity of Lanthanide Oxides for Different Coordination Numbers," *Physica B*, **403** [10] 1787-92 (2008).

30. A. Jaworski, B. Stevensson, B. Pahari, K. Okhotnikov, and M. Edén, "Local Structures and Al/Si Ordering in Lanthanum Aluminosilicate Glasses Explored by Advanced ^{27}Al NMR Experiments and Molecular Dynamics Simulations," *Phys. Chem. Chem. Phys.*, **14** [45] 15866-78 (2012).

31. J. Marchi, D. S. Morais, J. Schneider, J. C. Bressiani, and A. H. A. Bressiani, "Characterization of Rare Earth Aluminosilicate Glasses," *J. Non-Cryst. Solids*, **351** [10] 863-8 (2005).

32. S. Baghshahi, M. P. Brungs, C. C. Sorrell, and H. S. Kim, "Surface Crystallization of Rare-Earth Aluminosilicate Glasses," *J. Non-Cryst. Solids*, **290** [2] 208-15 (2001).

33. Y. B. Saddeek, K. A. Aly, A. Dahshan, and I. M. E. Kashef, "Optical Properties of the Na_2O-B_2O_3-Bi_2O_3-MoO_3Glasses," *J. Alloys Compd.*, **494** [1-2] 210-3 (2010).

34. J. McCloy, B. Riley, B. Johnson, M. Schweiger, H. A. Qiao, and N. Carlie, "The Predictive Power of Electronic Polarizability for Tailoring the Refractivity of High-Index Glasses: Optical Basicity Versus the Single Oscillator Model," *J. Am. Ceram. Soc.* **93** [6] 1650-62 (2010).

35. T. Schaller and J. F. Stebbins, "The Structural Role of Lanthanum and Yttrium in Aluminosilicate Glasses: A ^{27}Al and ^{17}O Mas NMR Study," *J. Phys. Chem. B*, **102** [52] 10690-7 (1998).

36. S. K. Lee and J. F. Stebbins, "The Structure of Aluminosilicate Glasses: High-Resolution ^{17}O and ^{27}Al MAS and 3QMAS NMR Study," *J. Phys. Chem. B*, **104** [17] 4091-100 (2000).

37. S. Sen and R. E. Youngman, "High-Resolution Multinuclear NMR Structural Study of Binary Aluminosilicate and Other Related Glasses," *J. Phys. Chem. B*, **108** [23] 7557-64 (2004).

38. I. J. Lowe, "Lowe, Irving J.: My Life in the Rotating Frame," *eMagRes.*, Edited by R. K. Harris and R. L. Wasylishen . John Wiley & Sons, Hoboken, NJ, 2007 DOI: 10.1002/9780470034590.emrhp0113.

39. E. R. Andrew, R. E. Richards, and K. J. Packer, "Magic Angle Spinning in Solid State N.M.R. Spectroscopy," *Philos. Trans. Royal Soc. A*, **299** [1452] 505-20 (1981).

40. S. Iftekhar, E. Leonova, and M. Edén, "Structural Characterization of Lanthanum Aluminosilicate Glasses by ^{29}Si Solid-State NMR," *J. Non-Cryst. Solids*, **355** [43-44] 2165-74 (2009).

41. M. v. Exter and D. Grischkowsky, "Optical and Electronic Properties of Doped Silicon from 0.1 to 2 Thz," *Appl. Phys. Lett*, **56** [17] 1694-6 (1990).

42. S. Kojima, H. Kitahara, S. Nishizawa, Y. S. Yang, and M. Wada Takeda, "Terahertz Time-Domain Spectroscopy of Low-Energy Excitations in Glasses," *J. Mol. Struct*, **744-747**, 243-6 (2005).

43. M. Naftaly and R. E. Miles, "Terahertz Time-Domain Spectroscopy: A New Tool for the Study of Glasses in the Far Infrared," *J. Non-Cryst. Solids*, **351** [40] 3341-6 (2005).

44. P. Y. Han, M. Tani, M. Usami, S. Kono, R. Kersting, and X.-C. Zhang, "A Direct Comparison between Terahertz Time-Domain Spectroscopy and Far-Infrared Fourier Transform Spectroscopy," *J. Appl. Phys.*, **89** [4] 2357-9 (2001).

45. M. Naftaly and R. E. Miles, "Terahertz Time-Domain Spectroscopy of Silicate Glasses and the Relationship to Material Properties," *J. Appl. Phys.*, **102** [4] 043517 (2007).

46. C. Yatongchai, A. W. Wren, and S. K. Sundaram, "Characterization of Hydroxyapatite-Glass Composites Using Terahertz Time-Domain Spectroscopy," *J. Infrared, Millimeter, Terahertz Waves,* **36** [1] 81-93 (2014).

47. H. Huang, L.-M. Yang, and J. Liu, "Femtosecond Fiber Laser Direct Writing of Optical Waveguide in Glasses," *Proc. SPIE,* **8164**, 81640B1-8 (2011)

48. S. K. Sundaram and E. Mazur, "Inducing and Probing Non-Thermal Transitions in Semiconductors Using Femtosecond Laser Pulses," *Nat. Mater.,* **1** [4] 217-24 (2002).

49. K. M. Davis, K. Miura, N. Sugimoto, and K. Hirao, "Writing Waveguides in Glass with a Femtosecond Laser," *Opt. Lett.,* **21** [21] 1729-31 (1996).

50. P. Florian, N. Sadiki, D. Massiot, and J. P. Coutures, "27-Al NMR Study of the Structure of Lanthanum and Yttrium Based Alumino-silicate Glasses and Melts," *J. Phys. Chem. B,* **111** [33] 9747-57 (2007).

51. A. Jaworski, B. Stevensson, B. Pahari, K. Okhotnikov, and M. Eden, "Local Structures and Al/Si Ordering in Lanthanum Aluminosilicate Glasses Explored by Advanced ^{27}Al NMR Experiments and Molecular Dynamics Simulations," *Phys. Chem.,* **14** [45] 15866-78 (2012).

52. D. R. Neuville, L. Cormier, and D. Massiot, "Al Environment in Tectosilicate and Peraluminous Glasses: A ^{27}Al MQ-MAS NMR, Raman, and Xanes Investigation," *Geochim. Cosmochim. Acta,* **68** [24] 5071-9 (2004).

53. A. Aronne, S. Esposito, and P. Pernice, "FTIR and DTA Study of Lanthanum Aluminosilicate Glasses," *Mater. Chem. Phys.,* **51** [2] 163-8 (1997).

54. R. Boscaino, E. Vella, and G. Navarra, "Absorption Edge in Silica Glass,*": pp.* 318-22 *Proceedings of 2005 IEEE/LEOS Workshop on Fibres and Optical Passive Components, 2005*. Edited by S. Riva-Sanseverino, M. Artiglia, IEEE, New York, 2005.

55. F. M. F, H. Mohamed Kamari, and A. M.N, "Effect of Lanthanum Oxide on Optical Properties of Zinc Borotellurite Glass System," *J. Optoelectronic and Biomedical Materials,* **8** [2] 49-59 (2016).

56. B. Bhatia, S. L. Meena, V. Parihar, and M. Poonia, "Optical Basicity and Polarizability of Nd^{3+} Doped Bismuth Borate Glasses," *New J. Glass Ceram.,* **52** [5] 44-52 (2015).

57. C. Karras, D. Litzkendorf, S. Grimm, K. Schuster, W. Paa, and H. Stafast, "Nonlinear Refractive Index Study on SiO_2- Al_2O_3-La_2O_3Glasses," *Opt. Mater. Express,* **4** [10] (2014).

58. M. Plucinski and J. W. Zwanziger, "Topological Constraints and the Makishima–Mackenzie Model," *J. Non-Cryst. Solids,* **429**, 20-3 (2015).

59. S. Keun, L. And, and J. F. Stebbins, "The Degree of Aluminum Avoidance in Aluminosilicate Glasses," *Am. Mineral.*, **84** [5] 937-45 (1999).

60. A. N. Gleizes, D. Samélor, C. Vahlas, V. Sarou-Kanian, P. Florian, and D. Massiot, "Temperature Dependent 4-, 5- and 6-Fold Coordination of Aluminum in MOCVD-Grown Amorphous Alumina Films: From Local Coordination to Material Properties," *Adv. Sci. Tech.*, **91** 123-33 (2014).

61. A. Herrmann, S. Kuhn, M. Tiegel, and C. Rüssel, "Fluorescence Properties of Eu^{3+}-Doped Aluminosilicate Glasses," *Opt. Mater.*, **37** 293-97 (2014).

62. U. Strom and P. C. Taylor, "Temperature and Frequency Dependences of the Far-Infrared and Microwave Optical Absorption in Amorphous Materials," *Phys. Rev. B,* **16** [12] 5512-22 (1977).